



**HAL**  
open science

## **miR-4510 blocks hepatocellular carcinoma development through RAF1 targeting and RAS/RAF/MEK/ERK signalling inactivation**

Amani Ghousein, Nicola Mosca, Flora Cartier, Justine Charpentier,  
Jean-William Dupuy, Anne-Aurélie Raymond, Paulette Bioulac-Sage,  
Christophe F Grosset

### ► To cite this version:

Amani Ghousein, Nicola Mosca, Flora Cartier, Justine Charpentier, Jean-William Dupuy, et al.. miR-4510 blocks hepatocellular carcinoma development through RAF1 targeting and RAS/RAF/MEK/ERK signalling inactivation. *Liver International*, 2019, 40 (1), pp.240-251. 10.1111/liv.14276 . inserm-02437915

**HAL Id: inserm-02437915**

**<https://inserm.hal.science/inserm-02437915>**

Submitted on 14 Jan 2020

**HAL** is a multi-disciplinary open access archive for the deposit and dissemination of scientific research documents, whether they are published or not. The documents may come from teaching and research institutions in France or abroad, or from public or private research centers.

L'archive ouverte pluridisciplinaire **HAL**, est destinée au dépôt et à la diffusion de documents scientifiques de niveau recherche, publiés ou non, émanant des établissements d'enseignement et de recherche français ou étrangers, des laboratoires publics ou privés.



**miR-4510 Blocks Hepatocellular Carcinoma Development  
Through RAF1 Targeting and RAS/RAF/MEK/ERK Signaling  
Inactivation**

|                               |  |
|-------------------------------|--|
| Journal:                      | <i>Liver International</i>   |
| Manuscript ID                 | LIVint-19-00426.R1   |
| Wiley - Manuscript type:      | Original Articles  |
| Date Submitted by the Author: | 20-Sep-2019  |
| Complete List of Authors:     | Ghousein, Amani; INSERM U1035, Biothérapies des Maladies Génétiques, Inflammatoires et Cancer<br>Mosca, Nicola; INSERM U1035, Biothérapies des Maladies Génétiques, Inflammatoires et Cancer<br>Cartier, Flora; INSERM U1035, Biothérapies des Maladies Génétiques, Inflammatoires et Cancer<br>Charpentier, Justine; INSERM U1035, Biothérapies des Maladies Génétiques, Inflammatoires et Cancer<br>Dupuy, Jean-William; Centre de Génomique Fonctionnelle de Bordeaux, Plateforme Proteome<br>Raymond, anne-aurélie; Université de Bordeaux, Inserm U1053<br>Bioulac-Sage, Paulette; Université Bordeaux, Inserm U1053<br>Grosset, Christophe; Université de Bordeaux, Inserm, BMGIC, U1035 |
| Keywords:                     | hepatocellular carcinoma, proteomic, RAF1, ERK Signaling, miR-4510   |
|                               |  |

SCHOLARONE™  
Manuscripts

# miR-4510 Blocks Hepatocellular Carcinoma Development Through *RAF1*

## Targeting and RAS/RAF/MEK/ERK Signaling Inactivation

Amani Ghousein,<sup>1</sup> Nicola Mosca,<sup>1</sup> Flora Cartier,<sup>1</sup> Justine Charpentier,<sup>1</sup> Jean-William Dupuy,<sup>2</sup> Anne-  
Aurélié Raymond,<sup>3,4</sup> Paulette Bioulac-Sage,<sup>3</sup> and Christophe F. Grosset<sup>1,5</sup>

<sup>1</sup>Univ. Bordeaux, Inserm, BMGIC, U1035, 33076 Bordeaux, France.

<sup>2</sup>Univ. Bordeaux, Centre de Génomique Fonctionnelle de Bordeaux, Plateforme Proteome, Bordeaux, France.

<sup>3</sup>Univ. Bordeaux, Inserm, BARITON, U1053, 33076 Bordeaux, France.

<sup>4</sup>ORCID ID: <http://orcid.org/0000-0003-2697-9352>

<sup>5</sup>ORCID ID: <https://orcid.org/0000-0002-0479-6291>

**Contact information** : Christophe F. Grosset, Université de Bordeaux, INSERM, BMGIC, U1035, 146, Rue Leo Saignat, 33076 Bordeaux Cedex, France; E-mail: [christophe.grosset@inserm.fr](mailto:christophe.grosset@inserm.fr); Tel.: +33 557 574 630; Fax: +33 557 571 374.

**Electronic word count**: 4998 words

**Total number of Figures and Tables**: 5

### Abbreviations

CAM, chorioallantoic membrane; CCNB1, Cyclin B1; CDK, cyclin-dependent kinase; CTRL, small RNA control; ERK, extracellular signal-regulated kinase; FOS, *c-Fos* proto-oncogene; GPC3, glypican-3; HCC,

1 hepatocellular carcinoma; miR-4510, mature microRNA-4510; miRNA, microRNA; mRNA, messenger RNA;  
2 NTL, nontumoral liver; RAF1, RAF proto-oncogene serine/threonine-protein kinase; SMARC, SWI/SNF-  
3 related matrix-associated actin-dependent regulator of chromatin; UTR, untranslated region.

4  
5 **Conflict of interest:** The authors declare that they have no conflict of interest.

#### 6 7 **Statement of financial support**

8 This study was supported by grants from L'Association pour le Développement du Liban to AG, La Ligue  
9 Régionale Contre le Cancer (Comités Dordogne; Comité Gironde) to AG and CFG, the French State in the  
10 framework of the "Investments for the future" Programme IdEx Bordeaux (grant ANR-10-IDEX-03-02) to  
11 NM and La region Nouvelle-Aquitaine to NM.

#### 12 13 **Acknowledgements**

14 We thank Véronique Guyonnet-Duperrat from the Vectorologie Platform of Bordeaux University and  
15 Francis Saggiocco for his helpful technical assistance. We also thank Jean-Max Pasquet for providing  
16 materials and Martin Hagedorn for critical comments on the manuscript. The flow cytometry and histology  
17 were done in the Cytometry and Histology platforms, respectively, two service units of the TBM Core and  
18 Bordeaux University.

#### 19 20 **Abstract**

21 **Background:** Therapeutic outcomes using the multikinase inhibitors sorafenib or regorafenib remain  
22 unsatisfactory for patients with advanced hepatocellular carcinoma (HCC). Thus, new drug modalities are  
23 needed. We recently reported the remarkable capacity of miR-4510 to impede the growth of HCC and  
24 hepatoblastoma through *Glypican-3* (GPC3) targeting and Wnt pathway inactivation. **Methods:** To identify

1  
2  
3 1 new targets of miR-4510, we used a label-free proteomic approach and reported down-regulation of RAF  
4  
5 2 proto-oncogene serine/threonine-protein kinase (RAF1) by miR-4510. Because the tumorigenic role of  
6  
7 3 RAF1 in HCC is controversial, we further studied *RAF1*:miR-4510 interactions using cellular, molecular as  
8  
9 4 well as functional approaches and a chicken chorioallantoic membrane (CAM) xenograft model. **Results:**  
10  
11 5 We found an increase in RAF1 protein in 59.3% of HCC patients and a specific up-regulation of its transcript  
12  
13 6 in proliferative tumors. We showed that miR-4510 inactivates the RAS/RAF/MEK/ERK pathway and  
14  
15 7 reduces the expression of downstream targets (i.e., c-Fos proto-oncogene [FOS]) through *RAF1* direct  
16  
17 8 targeting. At a cellular level, miR-4510 inhibited HCC cell proliferation and migration and induced  
18  
19 9 senescence in part by lowering RAF1 messenger RNA (mRNA) and protein expression. Finally, we  
20  
21 10 confirmed the pro-tumoral function of RAF1 protein in HCC cells and its ability to sustain HCC tumor  
22  
23 11 progression *in vitro* and *in vivo*. **Conclusions:** In this work we confirm that RAF1 acts as an oncogene in  
24  
25 12 HCC and further demonstrate that miR-4510 acts as a strong tumor suppressor in the liver by targeting  
26  
27 13 many proto-oncogenes, including *GPC3* and *RAF1*, and subsequently controlling key biological and  
28  
29 14 signaling pathways among which Wnt and RAS/RAF/MEK/ERK signals.  
30  
31  
32  
33  
34  
35  
36  
37  
38  
39  
40

16 **Keywords:** liver; hepatocellular carcinoma; miR-4510; RAF1; RAS/RAF/MEK/ERK signaling.

18 **Lay summary:**

19 We previously reported that miR-4510 acts as a powerful antitumor molecule. In this new work, we  
20 aimed to better understand how miR-4510 molecularly acts to inhibit liver tumor development. We found  
21 that miR-4510 limits the oncogenic effect of RAF1 protein by lowering its expression and its functional  
22 impact in liver cancer.

23

24

## 1 INTRODUCTION

2 With approximately 782,000 new cases diagnosed each year in the world, hepatocellular carcinoma  
3 (HCC) is the most frequent primary malignant liver tumor and is characterized by a very poor prognosis (5-  
4 year survival <15%), dismal outcomes, and a steadily increasing incidence [1]. The main risk factors for HCC  
5 are chronic liver diseases due to hepatotropic viruses (hepatitis B and C), alcohol consumption, and  
6 metabolic syndromes [1]. Only one-third of patients with stage 0-A tumor can benefit from middle-term  
7 curative regimens, including surgical resection, local ablation, and liver transplantation [1, 2]. For more  
8 advanced diseases, the only approved drugs are sorafenib and regorafenib, two multikinase inhibitors that  
9 increase patients' overall survival by approximately 3 months [3, 4]. Reasons for a failure of targeted  
10 chemotherapies in advanced HCC are various and partially known. Some might include the lack of clear  
11 driver-mutation identification in the treated population, complex molecular crosstalk between pro-  
12 oncogenic pathways, high intratumor heterogeneity, drug resistance, and underlying hepatic dysfunctions  
13 [1, 2]. Fortunately, many new drugs comprising immune checkpoint inhibitors, virus-based systems,  
14 inhibitors of Hepatocyte growth factor receptor (MET) and mammalian target of rapamycin (mTOR), or  
15 anti-angiogenic agents are currently under clinical evaluation for HCC [3, 4]. Future advances in HCC  
16 treatment likely reside in the combined use of multitarget drugs or therapeutic approaches (transarterial  
17 chemoembolization plus chemotherapy) [3, 4] and in the development of new drug delivery vehicles (e.g.,  
18 extracellular vesicles and nanoparticles) or smart pro-drugs presenting both high antitumor property and  
19 weak toxicity for the normal tissue compared to the uncoupled drugs [5, 6].

20 MicroRNAs (miRNAs) are short noncoding RNAs whose function is to post-transcriptionally regulate  
21 gene expression. miRNA-mediated regulation occurs through sequence-specific binding to the coding or  
22 untranslated regions (UTRs) of target messenger RNA (mRNA) [7, 8]. Thus, the miRNA-mRNA duplex  
23 formation triggers translational repression and/or deadenylation-dependent mRNA decay and ultimately  
24 reduces protein output. Approximately 2,500 miRNAs control thousands of genes involved in normal and

1  
2  
3 1 pathological biological processes, including development, differentiation, proliferation, migration,  
4  
5 2 inflammation, and tumorigenesis. Compelling evidences have implied miRNAs as true drivers of liver  
6  
7 3 tumorigenesis in HCC [7] and hepatoblastoma, a primary liver tumor in early childhood [9]. miRNAs finely  
8  
9 4 tune many cellular processes that are fundamental for normal hepatocytes or hepatoma cells [7, 10].  
10  
11 5 Although the effect mediated by one miRNA on any particular target is modest, the simultaneous  
12  
13 6 regulation of a broad array of transcripts can lead to profound phenotypical changes and gene  
14  
15 7 reprogramming [11, 12]. Due to their functional redundancy and multitargeting ability, adequately  
16  
17 8 formulated miRNAs might offer new therapeutic perspectives for patients presenting with advanced HCC  
18  
19 9 [1, 5, 11-13].  
20  
21  
22  
23

24 10 Recently, we reported for the first time the tumor-suppressive role of mature microRNA 4510 (miR-  
25  
26 11 4510) in both HCC and hepatoblastoma [10]. Our data showed that miR-4510 is decreased in hepatic  
27  
28 12 tumors, blocks the growth and proliferation of cancerous hepatic cells *in vitro* and *in vivo*, induces  
29  
30 13 apoptosis, and inhibits Wnt signaling and the expression of downstream targets, including *BMP4*, *DKK1*,  
31  
32 14 *LEF1*, and *TCF7L1*. The blocking of endogenous miR-4510 with a specific anti-miR also increased HCC cell  
33  
34 15 growth [10]. Part of the phenotypical changes mediated by miR-4510 in HCC cells was dependent on  
35  
36 16 *Glypican-3 (GPC3)* expression, the only validated miR-4510 target reported so far [10]. To gain further  
37  
38 17 insights into the tumor-suppressive role of miR-4510 in the liver, we sought to find new targets of this  
39  
40 18 miRNA using a label-free proteomic approach. After validating the decreased expression of several  
41  
42 19 oncogenes by miR-4510, we focused our interest on RAF proto-oncogene serine/threonine-protein kinase  
43  
44 20 (RAF1, also known as C-RAF), an intermediate member of the mitogen-activated protein  
45  
46 21 kinase/extracellular signal-regulated kinase (MAPK/ERK) signaling pathway (also known as  
47  
48 22 RAS/RAF/MEK/ERK pathway) with controversial oncogenic function in HCC [14-18]. We report the direct  
49  
50 23 regulation of RAF1 by miR-4510 in HCC cells and further confirm the oncogenic property of this  
51  
52 24 serine/threonine kinase in the pathogenesis of HCC.  
53  
54  
55  
56  
57  
58  
59  
60

## 1        1    **METHODS**

### 2        2    **Patient samples**

3                    Tissues were snap frozen and stored at  $-80^{\circ}\text{C}$ . Samples were obtained with written informed  
4                    consent, and the study protocol was approved by the ethics committee of Bordeaux Liver Bank (project  
5                    #BB-0033-00036). Liver samples were clinically, histologically, and genetically characterized (Supporting  
6                    Table S1). Liver tissues were immediately frozen in liquid nitrogen and stored at  $-80^{\circ}\text{C}$  until used for  
7                    molecular studies.

### 8                    9    **Cell culture, lentiviral transduction, and transfection by small RNAs**

10                    Human HCC-derived cell lines Huh7 and Hep3B were cultured in Dulbecco's modified Eagle's  
11                    medium (DMEM) (4.5 g/L; Invitrogen, Carlsbad, CA, USA), supplemented with 10% fetal bovine serum,  
12                    100 U/mL penicillin, and 100  $\mu\text{g}/\text{mL}$  streptomycin, maintained at  $37^{\circ}\text{C}$  in a humidified atmosphere of 5%  
13                     $\text{CO}_2$ , and harvested with 0.05% trypsin-0.03% ethylene diamine tetra-acetic acid (EDTA) [19]. Cell line  
14                    authentication was performed every year using short tandem repeat analysis, and absence of mycoplasma  
15                    contamination in cell culture media was tested every month. Stable Huh7 cells coexpressing tomato  
16                    transgene and green fluorescent protein (GFP) transgene harboring the wild-type (WT) or mutated (MUT)  
17                    *RAF-1* 3'-UTR were generated by lentiviral transduction using a multiplicity of infection (MOI) of 1. Stable  
18                    Huh7 and Hep3B cells expressing human RAF1 were generated by lentiviral transduction using an MOI of  
19                    5. Production and titration of infectious lentiviral particles, cell transduction, as well as biosafety  
20                    considerations and procedures have been described [19]. Cell transfections were done as described [20]  
21                    using the following small RNAs: miR-4510 mimic as well as small interfering RNA against RAF1 (siRAF1)  
22                    (Sigma-Aldrich, St Louis, MO, USA) and AllStars Negative Control small interfering RNA (siRNA) (Qiagen,  
23                    Hilden, Germany).

24

## 1 **Sample preparation for proteomic analysis**

2 This analysis was performed by the proteomics core facility at University of Bordeaux. The steps of  
3 sample preparation and protein digestion were performed as described [21].  
4

## 5 **Nano liquid chromatography–tandem mass spectrometry analysis**

6 Online nano liquid chromatography–tandem mass spectrometry (LC-MS/MS) analyses were  
7 performed using an Ultimate 3000 RSLC Nano-UPHLC system (Thermo Scientific, USA) coupled to a  
8 nanospray Q Exactive hybrid quadrupole-Orbitrap mass spectrometer (Thermo Scientific, USA). Then, 500  
9 ng of each peptide extract was loaded on a 300- $\mu$ m ID x 5 mm PepMap C18 precolumn (Thermo Scientific,  
10 USA) at a flow rate of 10  $\mu$ L/minute. After a 3-minute desalting step, peptides were separated on a 75- $\mu$ m  
11 ID x 25 cm C18 Acclaim PepMap RSLC column (Thermo Scientific, USA) with a 4% to 40% linear gradient of  
12 solvent B (0.1% formic acid in 80% acetonitrile) for 108 minutes. The separation flow rate was set to 300  
13 nL/minute. The mass spectrometer operated in positive ion mode at a 1.8-kV needle voltage. Data were  
14 acquired using Xcalibur 3.1 software in a data-dependent mode. MS scans ( $m/z$  300-1600) were recorded  
15 at a resolution of  $R = 70000$  (at  $m/z$  200) and an Automatic gain control (AGC) target of  $3 \times 10^6$  ions  
16 collected within 100 ms. Dynamic exclusion was set to 30 seconds, and top 12 ions were selected from  
17 fragmentation in higher-energy C-trap dissociation (HCD) mode. MS/MS scans with a target value of  $1 \times$   
18 105 ions were collected with a maximum fill time of 100 ms and a resolution of  $R = 17500$ . Additionally,  
19 only +2 and +3 charged ions were selected for fragmentation. Other settings included no sheath and no  
20 auxiliary gas flow; heated capillary temperature, 200°C; normalized HCD collision energy of 27 eV; and an  
21 isolation width of 2  $m/z$ .  
22

## 23 **Database search and processing**

1  
2  
3 1 For protein identification, Sequest HT and Mascot 2.4 algorithms through Proteome Discoverer 1.4  
4  
5 2 Software (Thermo Fisher Scientific, Inc.) were used for protein identification in batch mode by searching  
6  
7 3 against a *Homo sapiens* protein database (68,421 entries, Reference Proteome Set , release 2015\_04;  
8  
9 4 <http://www.uniprot.org/website>). Two missed enzyme cleavages were allowed. Mass tolerances in MS  
10  
11 5 and MS/MS were set to 10 ppm and 0.02 Da. Oxidation of methionine, acetylation of lysine, and  
12  
13 6 deamidation of asparagine and glutamine were searched as dynamic modifications.  
14  
15 7 Carbamidomethylation on cysteine was searched as static modification. Peptide validation was performed  
16  
17 8 using Percolator algorithm, and only “high confidence” peptides were retained corresponding to a 1% false  
18  
19 9 discovery rate (FDR) at peptide level [22].  
20  
21  
22  
23  
24  
25  
26

### 27 11 **Label-Free Quantitative Data Analysis**

28  
29 12 Raw LC-MS/MS data were imported in Progenesis Q1 (version 2.0; Nonlinear Dynamics, a Waters  
30  
31 13 Company) for feature detection, alignment, and quantification. All sample features were aligned according  
32  
33 14 to retention times by manually inserting up to 50 landmarks followed by automatic alignment to maximally  
34  
35 15 overlay all the 2-dimensional (m/z and retention time) feature maps. Singly charged ions and ions with  
36  
37 16 higher charge states than 6 were excluded from analysis. All remaining features were used to calculate a  
38  
39 17 normalization factor for each sample that corrects for experimental variation. Peptide identifications (with  
40  
41 18 FDR <1%) were imported into Progenesis. Only nonconflicting features and unique peptides were  
42  
43 19 considered for calculation of quantification at protein level. A minimum of two peptides matched to a  
44  
45 20 protein was used as the criterion for identification as a differentially expressed protein. We applied a *t* test  
46  
47 21 (Welch’s *t* test that does not assume equal population variance) to miR-4510 versus control. We set the  
48  
49 22 threshold for the significance of the adjusted *P* value at 0.05. The MS proteomics data have been deposited  
50  
51 23 to the ProteomeXchange Consortium through the PRIDE [23] partner repository with the data set identifier  
52  
53 24 PXD010085.  
54  
55  
56  
57  
58  
59  
60

1  
2  
3 1  
45 2 **Antibodies, immunoblot analysis**  
6

7 3 Cells were lysed in RIPA lysis buffer (Sigma, St Louis, MO, USA) supplemented with protease inhibitor  
8 4 cocktail (Roche Diagnostics, Mannheim, Germany), and protein concentration was determined using the  
9 5 Pierce BCA Protein Assay Kit (Thermo Scientific, Rockford, USA). Approximately 40 µg of proteins from  
10 6 each sample were separated on 4% to 15% precast polyacrylamide gel (Bio-Rad, Hercules, CA, USA) and  
11 7 blotted onto nitrocellulose membranes (0.2 µm nitrocellulose, Bio-Rad) using Trans-Blot Turbo Transfer  
12 8 System (Bio-Rad). The membranes were blocked in 5% skim milk and then incubated with each of the  
13 9 following specific primary antibodies: rabbit anti-cyclin-dependent kinase 6 (CDK6) (1:1000, SC-177, Santa  
14 10 Cruz Biotechnology); rabbit anti- S-phase kinase-associated protein 2 (SKP2) (1:1000, #4358, Cell Signaling  
15 11 Technology); rabbit anti-cyclin B1 (CCNB1) (1:1000, GTX100911, Gene Tex); mouse anti-RAF1 (1:1000, SC-  
16 12 7267, Santa Cruz Biotechnology); mouse anti-ERK (1:2000, #4696, Cell Signaling Technology); rabbit anti-  
17 13 phospho-ERK (p-ERK) (1:1000, #4377, Cell Signaling Technology); rabbit anti-CFOS (1:1000, SC-52, Santa  
18 14 Cruz Biotechnology); mouse anti-Myc proto-oncogene protein (MYC) (1:1000, SC-40, Santa Cruz  
19 15 Biotechnology); mouse anti-GPC3 (1:1000, B0025R, Biomosaics); and rabbit anti-glyceraldehyde 3-  
20 16 phosphate dehydrogenase [GAPDH] (1:2000, SC-25778, Santa Cruz Biotechnology) at 4°C overnight. All  
21 17 blots were analyzed with the Odyssey system (Li-Cor Biosciences).

18  
1920 19 **Chick chorioallantoic membrane assay**  
21

22 20 Fertilized embryos were received at the stage of segmentation and then incubated at 37.4°C and 70%  
23 21 humidity. At day 3 of development, the eggshell was opened on the top and the opening sealed with  
24 22 medical-grade Durapore tape. At day 10 of embryonic development, 1 million Huh7 cells were embedded  
25 23 in Matrigel (growth-factor reduced, Corning, Corning, NY, USA) droplets (40 µL) and deposited on the  
26 24 chorioallantoic membrane (CAM). Pictures of experimental tumors were taken every day (until day 16 of

1 embryonic development) using a stereomicroscope (SMZ745T) and camera (DS-Fi2) from Nikon and then  
2 analyzed with the NSI Element D software (Nikon, Tokyo, Japan). At day 16 of embryonic development, all  
3 tumors were formalin-fixed and weighed using a precision balance after they were further processed for  
4 histology.

## 6 **Bioinformatic and statistical analyses**

7 miR-4510 target selection was done using a score  $>-0.3$  for TargetScan 7.2 [24] and a seed match = 1 and  
8 an energy  $<-22.0$  for miRWalk 3.0 (<http://mirwalk.umm.uni-heidelberg.de>) [25]. All data are displayed as  
9 a mean of three or more independent experiments, and error bars indicate standard deviation of the  
10 mean. Statistical analyses were performed using GraphPad Prism 5.0 or 6.0 software as described [10].  
11 When an experiment contained two unmatched groups of values, the nonparametric Mann-Whitney test  
12 was used for the comparison of means. When an experiment contained two paired groups, the 2-tailed  
13 Wilcoxon matched-pairs signed ranked test was used. When an experiment contained three groups of  
14 values or more, regular one-way or two-way analysis of variance (ANOVA) was used for the comparison  
15 of multiple means. The one-way ANOVA test was followed by the Dunnett's multiple-comparison post-  
16 test when all data were compared to control or by the Bonferroni's multiple-comparison post-test when  
17 all data were compared. The two-way ANOVA test was followed by the Tuckey's multiple-comparison post-  
18 test when all data were compared to control. The *P* value is indicated at the bottom of each figure legend.  
19 In each figure, the number of independent experiments (*n*) and the ANOVA *P* value is indicated in brackets.  
20 Results were considered significant when  $P < 0.05$ . For all data in figures: \* $P < 0.05$ ; \*\* $P < 0.01$ ; \*\*\* $P <$   
21 0.001.  
22 See supporting Materials and Methods for additional details.

## 1 RESULTS

### 2 Identification of new targets of miR-4510 in HCC cells

3 To find new targets of miR-4510, we transfected HCC-derived Huh7 cells with a synthetic miR-4510  
4 mimic or a small RNA control (CTRL), extracted total proteins 24 hours later, and comparatively analyzed  
5 cellular proteomes using a label-free approach. LC-MS/MS spectra analyses detected 3,300 proteins and,  
6 according to a reproducible up- or down-regulation of 25% or more (with ratio  $\geq 2$  or  $\leq 0.5$ ), revealed 611  
7 significantly deregulated proteins (322 down and 289 up) in miR-4510-transfected cells compared to  
8 control cells (Fig. 1a; Supporting Tables S2 and S3). Among the 322 down-regulated proteins and possible  
9 novel miR-4510 targets, 54 (TargetScan 7.2 [24]) and 23 (miRWalk 3.0 [25]) genes encoding for these  
10 proteins were highly predicted to interact with miR-4510, and 9 genes (*DRG2*, *GPI*, *LASP1*, *LIG3*, *RAB1B*,  
11 *RAF1*, *RTN3*, *TPP1*, *UQCC1*) were collectively found in proteomic data and mRNA:miRNA predictions (see  
12 insert in Fig. 1a). Noticeably, many of the 322 decreased proteins are associated with cell cycle,  
13 proliferation, survival, signaling, protein synthesis, metabolic pathways (lipids; amino and nucleic acids),  
14 and genome regulation (Fig. 1b). The down-regulation of CDK6, S-phase kinase-associated protein 2  
15 (SKP2), G2/mitotic-specific cyclin B1 (CCNB1), and RAF1 proteins in miR-4510-transfected cells was  
16 confirmed by western blot (Fig. 1c), therefore validating our proteomic data (Fig. 1a). We previously  
17 showed that miR-4510 inhibits cell proliferation by arresting HCC cells in G0 and reducing their entry in S  
18 phase [10]. Therefore, miR-4510 likely exerts its anti-proliferative function through the direct or indirect  
19 down-regulation of CDK6, SKP2, and CCNB1. We also noticed that RAF1 was involved in many cellular and  
20 molecular processes altered in miR-4510-transfected Huh7 cells (Fig. 1b; Supporting Table S4), suggesting  
21 a central role of this serine/threonine-protein kinase in miR-4510 tumor-suppressive function. Altogether,  
22 our results show that miR-4510 controls a large spectrum of genes in hepatic cells and decreases  
23 expression of multiple well-known oncogenes, some comprising cell cycling effectors and cell signaling  
24 mediators, among which RAF1 stands as a key effector.

1  
2  
3 1  
4  
5 2

## Deregulation of RAF1 in HCC

3        *RAF1* encodes for the serine/threonine kinase RAF1 with intermediate regulatory functions in the  
4 linear RAS/RAF/MEK/ERK pathway. Because RAF1 overexpression in HCC was still a matter of debate [14-  
5 16], we measured its expression by western blot using total protein extracts from 27 patient samples  
6 (Supporting Fig. S1) [10]. In our cohort, RAF1 protein was globally and significantly increased in HCC  
7 compared to nontumoral liver (NTL) (Fig. 2a). Paired tumor/NTL ratios highlighted that RAF1 is  
8 overexpressed in 16 samples (59.3%), unchanged in 10 samples (37.0%), and decreased in 1 sample (3.7%)  
9 (Fig. 2b). Disparity in RAF1 expression was also observed at a histological level using tissue sections from  
10 a total of 9 patients, and cirrhotic tissues were sometimes stained with RAF1 protein (Fig. 2c; Supporting  
11 Fig. S2), a result in agreement with a previous study [26]. Using publicly available transcriptomic data [27],  
12 we also found a specific increase in *RAF1* mRNA in proliferative HCC subgroups (G1, G3, and to a lesser  
13 extend G2; 35.7%) (Fig. 2d). Moreover, using the Human Protein Atlas databank  
14 ([www.proteinatlas.org/ENSG00000132155-RAF1](http://www.proteinatlas.org/ENSG00000132155-RAF1)), we found low expression of RAF1 protein in normal  
15 liver tissue and a staining of hepatocyte nuclei. The transcriptomic analysis of a cohort of 365 cases  
16 ([www.proteinatlas.org/ENSG00000132155-RAF1/pathology/tissue/liver+cancer#](http://www.proteinatlas.org/ENSG00000132155-RAF1/pathology/tissue/liver+cancer#)) with the best  
17 separation (comprising the first quartile of tumors) showed a significant association ( $P = 0.00266$ ) between  
18 high expression level of *RAF1* mRNA and poor survival of patients. Finally, correlation analysis of our cohort  
19 of samples showed that RAF1 protein expression inversely correlates with miR-4510 (Fig. 2e). Altogether,  
20 these data suggest that RAF1 expression is increased in a majority of HCC tumors, associated with poor  
21 prognosis probably due to a decrease of miR-4510.

## miR-4510 inhibits the RAS/RAF/MEK/ERK pathway by targeting *RAF1*

1  
2  
3 1 To further study the impact of miR-4510 on RAF1 and RAS/RAF/MEK/ERK signaling, we measured  
4  
5 2 the expression of ERK, phospho-ERK, and the downstream targets FOS and MYC in Huh7 cells.  
6  
7 3 Complementary experiments were performed with cells transfected with an siRNA specifically silencing  
8  
9 4 *RAF1*. Results clearly showed that consecutively to a strong decrease of *RAF1* mRNA (Fig. 3d) and protein  
10  
11 5 levels (Fig. 3a), miR-4510 triggered a dephosphorylation of ERK and a decline of FOS and MYC proto-  
12  
13 6 oncogene proteins (Fig. 3a-c). Similar results were observed with *RAF1* siRNA (Fig. 3a-d). miR-4510 and  
14  
15 7 siRAF1 also dramatically decreased RAF1 expression in Hep3B, a second HCC cell line (Supporting Fig. S3).  
16  
17 8 To determine whether miR-4510 directly interacts with *RAF1* 3'-UTR, functional analyses were performed  
18  
19 9 using the fluorescent-reporter FunREG system [19, 20]. The predicted miR-4510 site located at position  
20  
21 10 219-225 in *RAF1* 3'-UTR was mutated by changing two cytidines in two guanines (r.221C>G and r.223C>G;  
22  
23 11 Fig. 3e). Compared to cells expressing eGFP-WT *RAF1* 3'-UTR transgene, these two base mutations totally  
24  
25 12 abolished the regulation of the fluorescent reporter gene by miR-4510 (Fig. 3e). Altogether, these data  
26  
27 13 demonstrated that miR-4510 inactivates RAS/RAF/MEK/ERK pathway in HCC cells by directly targeting  
28  
29 14 *RAF1* 3'-UTR at position 219-225.  
30  
31  
32  
33  
34  
35  
36

### 16 ***RAF1* silencing phenocopies miR-4510-mediated antitumor effect in HCC cells**

37  
38  
39 17 Because the oncogenic function of *RAF1* in HCC was controversial [14-16], we investigated the  
40  
41 18 impact of *RAF1* silencing in HCC cells using *in vitro* and *in vivo* approaches. Here, miR-4510 was used as  
42  
43 19 positive control for both cell growth inhibition and apoptosis induction [10]. *RAF1* silencing decreased the  
44  
45 20 growing capacity of both Huh7 and Hep3B cells by slightly extending the G0/G1 phase and shortening the  
46  
47 21 S phase (Fig. 4a-b; Supporting Fig. S4). As expected, similar but stronger effects were observed with miR-  
48  
49 22 4510. Moreover, both *RAF1* depletion and miR-4510 induced HCC cell senescence more efficiently than  
50  
51 23 the pro-senescent miRNA miR-624-5p [9], (Fig. 4c; Supporting Fig. S5) whereas only miR-4510 triggered  
52  
53 24 apoptosis in the two cell lines (Supporting Fig. S6). Interestingly, the combination of miR-4510 and  
54  
55  
56  
57  
58  
59  
60

1  
2  
3 1 sorafenib was more efficient to induce cell apoptosis than miR-4510 or sorafenib alone, and sorafenib  
4  
5 2 induced both miR-4510 increase and RAF1 protein reduction (Supporting Fig. S7). RAF1 silencing and miR-  
6  
7 3 4510 also significantly impeded the capacity of Huh7 cells to migrate (Fig. 4d; Supporting Fig. S8a-b). Next,  
8  
9 4 we investigated the impact of overexpressing a 3'-UTR-less *RAF1* transgene in HCC cells (Supporting Figs.  
10  
11 5 S9 and S10) and found that RAF1 potentiates the growth of both Huh7 and Hep3B cells (Fig. 4e). In  
12  
13 6 addition, overexpression of RAF1 partly counteracted the anti-proliferation effect of miR-4510 in both cell  
14  
15 7 lines (Fig. 4e). Altogether, these data show that the tumor-suppressive role of miR-4510 is partly mediated  
16  
17 8 by RAF1 targeting and down-regulation.  
18  
19  
20  
21  
22

### 23 10 ***RAF1* favors HCC tumor growth *in vivo***

24  
25 11 Next, we investigated the impact of RAF1 depletion on HCC growth *in vivo* using chicken embryos  
26  
27 12 presented by the tumor CAM model (Fig. 5a) [9, 10, 28]. At a macroscopic level, either before or after  
28  
29 13 tumor extraction and formalin fixation, we noticed that engrafted Huh7 cells formed a tissue mass smaller  
30  
31 14 with siRAF1 compared to control in 6 days with no bleeding (Fig. 5b, lanes 1 and 2). This observation was  
32  
33 15 further confirmed by weighting resected tumors (Fig. 5c) and measuring tumor thickness using formalin-  
34  
35 16 fixed paraffin-embedded hematoxylin-eosin-saffron (HES)-stained tissue sections (Fig. 5b, middle lane; Fig.  
36  
37 17 5d; Supporting Fig. S11a-b). After 6 days of tumor development, the decrease of RAF1 staining in siRAF1  
38  
39 18 tumors compared to control was confirmed by histology (Fig. 5b, lane 4; Supporting Fig. S11c-d). Similar  
40  
41 19 growth inhibition and histological data were obtained in miR-4510 tumors compared to control [10], (Fig.  
42  
43 20 5e; Supporting Fig. S12a-d) confirming the RAF1 inhibitory ability of miR-4510 in this animal model.  
44  
45 21 Moreover, the concomitant decrease of Ki67 immunostaining in siRAF1 tumors compared to control (Fig.  
46  
47 22 5b, bottom lane; Supporting Fig. S11e-f) showed that tumor cells were less abundant and less proliferative  
48  
49 23 following RAF1 silencing. Altogether, these data demonstrate that *RAF1* acts as an oncogene in HCC and  
50  
51 24 supports tumoral hepatic cell growth *in vivo*.  
52  
53  
54  
55  
56  
57  
58  
59  
60

## 1 DISCUSSION

2 We recently reported the decrease of miR-4510 in pediatric and adult liver cancers and its antitumor  
3 action through *GPC3* regulation and Wnt pathway inactivation [10]. miR-4510 was also found to be down-  
4 regulated in other malignancies, including bladder carcinoma [29], recurrent breast cancer [30], and  
5 colorectal adenocarcinoma [31]. Therefore, the decrease of miR-4510 in a broad variety of cancers points  
6 to its role as a general tumor suppressor. However, the only validated (oncogenic) target of miR-4510 is,  
7 so far, *GPC3* [10]. Here, we report that miR-4510 inhibits the RAS/RAF/MEK/ERK pathway in HCC cells by  
8 directly targeting *RAF1* through a site located in its 3'-UTR. Two additional miR-4510 sites were predicted  
9 to be located in *RAF1* 5'-UTR (Supporting Fig. S13), explaining in part the very strong inhibitory effect of  
10 miR-4510 on *RAF1* mRNA and protein expression (Fig. 3a,d; Supporting Fig. S3). However, the biological  
11 relevance of these sites was not tested in this work. Thus, these new data further confirm the antitumor  
12 function of miR-4510 and its role as a negative regulator of cellular functions (e.g., proliferation, survival,  
13 migration) through diminution of oncogenic signaling pathways among which Wnt/beta-catenin and  
14 RAS/RAF/MEK/ERK pathways. In addition, the down-regulation of CDK6, SKP2, and cyclin B1 proteins (and,  
15 to a lesser extent, GAK, CDK2, and CDK1; Supporting Table S2) in miR-4510-transfected Huh7 cells explains  
16 the strong and wide negative impact of miR-4510 *in vitro* and *in vivo* on both cell proliferation and cell  
17 cycling (Fig. 4) [10]. However, none of these genes was highly predicted to directly interact with miR-4510  
18 using TargetScan (data not shown). Additional oncogenes down-regulated by miR-4510 comprise SKP2, an  
19 E3 ubiquitin ligase that participates in cell survival by lowering the susceptibility of tumor cells to MYC-  
20 induced apoptosis [32], and SRPK1 (SRSF protein kinase 1), a splicing kinase involved in transcript  
21 maturation, which participates in tumor angiogenesis, invasiveness, and progression [33]. Several  
22 SWI/SNF-related, matrix-associated, actin-dependent regulator of chromatin (SMARC) proteins (e.g.,  
23 SMARCC2 and SMARCD1 and, to a lesser extent, SMARCA4, SMARCC1, and SMARCE1; Supporting Table  
24 S2) were also decreased in miR-4510-transfected Huh7 cells, suggesting a probable link between miR-

1  
2  
3 1 4510, SWI/SNF complex, and chromatin remodeling. In the literature, SMARCD1 is documented as a  
4  
5 2 tumorigenic and metastatic protein in gastric cancer [34], and it prevents cellular senescence and lipid  
6  
7 3 accumulation in hepatocytes [35]. Intriguingly, numerous SMARC members are increased in  
8  
9 4 hepatoblastoma and more particularly in proliferative and Fanconi Anemia pathway-activated C2A tumors  
10  
11 5 [36]. Therefore, it is likely that the marked pro-senescent effect of miR-4510 observed in HCC cells (Fig. 4c)  
12  
13 6 is linked to its capacity to control SMARCC2, SMARCD1, and SWI/SNF complex activation.  
14  
15

16 7 The serine/threonine kinase RAF1 is an intermediate component of the RAS/RAF/MEK/ERK pathway  
17  
18 8 cascade (also known as MAPK/ERK pathway) and serves as a link between ligand-activated receptor  
19  
20 9 tyrosine kinases (e.g., epidermal growth factor receptor [EGFR], fibroblast growth factor receptor [FGFR],  
21  
22 10 platelet-derived growth factor receptor [PDGFR]) and nuclear gene reprogramming that modulates  
23  
24 11 hundreds of genes, including many protumoral transcriptional factors (e.g., MYC, FOS). Alterations of  
25  
26 12 RAS/RAF/MEK/ERK pathway, mostly due to activating mutations in *RAS* and *BRAF* genes, have been  
27  
28 13 documented in many solid tumors, including HCC, melanoma, and lung, colon, and prostate carcinomas as  
29  
30 14 well as hematological malignancies such as myeloid leukemia [1, 17, 37]. Because of its central position in  
31  
32 15 RAS/RAF/MEK/ERK pathway, *RAF1* is tightly controlled in cells by both  
33  
34 16 phosphorylation/dephosphorylation mechanisms [17, 38] and miRNAs (e.g., miR-7-5p, miR-15a/b, miR-16,  
35  
36 17 and miR-195) [39, 40]. Thus, the regulation of *RAF1* by miR-4510 has several cellular and  
37  
38 18 pathophysiological implications. First, *RAF1* silencing by miR-4510 partly explains the remarkable  
39  
40 19 antitumor effect of miR-4510 on hepatic cancer cells [10]. Second, because sorafenib- or regorafenib-  
41  
42 20 based therapies are not curative and only slightly increase patient life expectancy, patients with advanced  
43  
44 21 HCC who need alternative therapeutic solutions may benefit from a miR-4510-based therapy. In addition,  
45  
46 22 many mechanisms of resistance have been experienced in relapsed patients following treatment with  
47  
48 23 *RAF1*, MEK, or ERK inhibitors [38], emphasizing the need to combine multikinase inhibitors with other  
49  
50 24 categories of antitumor agents to block multiple oncogenic pathways at the same time. Finally, our *in vitro*  
51  
52  
53  
54  
55  
56  
57  
58  
59  
60

1  
2  
3 1 data show that sorafenib provoked miR-4510 increase and RAF1 depletion. Moreover, the combination of  
4  
5 2 miR-4510 and sorafenib was more efficient to eliminate HCC cells compared to each molecule used alone  
6  
7 3 (Supporting Fig. S7). These data further confirm that sorafenib targets other kinases than RAF1 in cells and  
8  
9  
10 4 support the idea that combining miR-4510 with sorafenib or regorafenib may resolve current limitations  
11  
12 5 due to chemoresistance and poor responsiveness of patients with advanced HCC [1].  
13

14 6 Sorafenib is the standard of care for patients with advanced HCC, but unexpectedly, the dogma  
15  
16 7 about the oncogenic role of RAF1 in cancer was challenged by the study of Jeric and coworkers [14]. The  
17  
18 8 study showed that RAF1 is significantly down-regulated in HCC and negatively regulates liver  
19  
20 9 carcinogenesis and HCC cell proliferation [14]. Here, we provide evidence that *RAF1* mRNA is specifically  
21  
22 10 increased in proliferative and poor-prognosis HCC displaying *TP53* mutation, *CDKN2A* promoter  
23  
24 11 methylation, and chromosome instability [27] (Fig. 2d) In a cohort of non-selected 27 paired tumor/NTL  
25  
26 12 samples, we also found that RAF1 protein is increased in 59.3% of patients, unchanged in 37.0%, and  
27  
28 13 decreased in 3.7% (Fig. 2b). Data from the Human Protein Atlas databank further support our results and  
29  
30 14 report a weak expression of RAF1 protein in normal liver and a poor survival of HCC patients expressing  
31  
32 15 high level of RAF1. Finally, a study performed in Asian populations reported the up-regulation of RAF1  
33  
34 16 protein in 42.9% of liver cirrhosis and in 49.0% to 100% of HCC [26, 41]. Altogether, these data demonstrate  
35  
36 17 that (1) RAF1 expression is highly increased in HCC but variable from one patient to another, and (2) high  
37  
38 18 expression of RAF1 is associated with cell proliferation, chemoresistance, and tumor aggressiveness.  
39  
40 19 Therefore, any drug capable of blocking its expression and downstream biological pathways may be  
41  
42 20 beneficial to patients with advanced HCC, and miR-4510 stands as a significant candidate. The discrepancy  
43  
44 21 between our data and the work by Jeric and coworkers [14] remains unexplained at this stage and may be  
45  
46 22 due to the use of different cell types, animal models, and anti-RAF1 siRNAs.  
47  
48  
49  
50  
51

52 23 In conclusion, our work confirms the oncogenic function of RAF1 in HCC and further highlights the  
53  
54 24 remarkable antitumor function of miR-4510 in HCC and its central position in the control of cell  
55  
56  
57  
58  
59  
60

1  
2  
3 1 proliferation, survival, and mobility, making miR-4510 particularly relevant for miRNA-based therapies in  
4  
5 2 patients presenting advanced, unresectable, or drug-resistant liver cancer.  
6  
7  
8 3  
9  
10  
11  
12  
13  
14  
15  
16  
17  
18  
19  
20  
21  
22  
23  
24  
25  
26  
27  
28  
29  
30  
31  
32  
33  
34  
35  
36  
37  
38  
39  
40  
41  
42  
43  
44  
45  
46  
47  
48  
49  
50  
51  
52  
53  
54  
55  
56  
57  
58  
59  
60

Accepted version

1  
2  
3 1 REFERENCES  
4

- 5 2 1. Llovet, J.M., et al., *Advances in targeted therapies for hepatocellular carcinoma in the*  
6 3 *genomic era*. Nat Rev Clin Oncol, 2015.
- 7 4 2. Attwa, M.H. and S.A. El-Etreby, *Guide for diagnosis and treatment of hepatocellular*  
8 5 *carcinoma*. World J Hepatol, 2015. **7**(12): p. 1632-51.
- 9 6 3. Sherman, M., *Regorafenib for treatment of hepatocellular carcinoma*. Hepatology,  
10 7 2018. **67**(3): p. 1162-1165.
- 11 8 4. Ding, X.X., et al., *Precision medicine for hepatocellular carcinoma: driver mutations and*  
12 9 *targeted therapy*. Oncotarget, 2017. **8**(33): p. 55715-55730.
- 13 10 5. Varshosaz, J. and M. Farzan, *Nanoparticles for targeted delivery of therapeutics and*  
14 11 *small interfering RNAs in hepatocellular carcinoma*. World J Gastroenterol, 2015.  
15 12 **21**(42): p. 12022-41.
- 16 13 6. Renoux, B., et al., *Targeting the tumour microenvironment with an enzyme-responsive*  
17 14 *drug delivery system for the efficient therapy of breast and pancreatic cancers*. Chem  
18 15 *Sci*, 2017. **8**(5): p. 3427-3433.
- 19 16 7. Wang, X.W., N.H. Heegaard, and H. Orum, *MicroRNAs in liver disease*. Gastroenterology,  
20 17 2012. **142**(7): p. 1431-43.
- 21 18 8. Helwak, A., et al., *Mapping the human miRNA interactome by CLASH reveals frequent*  
22 19 *noncanonical binding*. Cell, 2013. **153**(3): p. 654-65.
- 23 20 9. Indersie, E., et al., *MicroRNA therapy inhibits hepatoblastoma growth in vivo by*  
24 21 *targeting beta-catenin and Wnt signaling*. Hepatol Commun, 2017. **1**(2): p. 168-183.
- 25 22 10. Cartier, F., et al., *New tumor suppressor microRNAs target glypican-3 in human liver*  
26 23 *cancer*. Oncotarget, 2017. **8**(25): p. 41211-41226.
- 27 24 11. Hayes, J., P.P. Peruzzi, and S. Lawler, *MicroRNAs in cancer: biomarkers, functions and*  
28 25 *therapy*. Trends Mol Med, 2014. **20**(8): p. 460-9.
- 29 26 12. Li, Z. and T.M. Rana, *Therapeutic targeting of microRNAs: current status and future*  
30 27 *challenges*. Nat Rev Drug Discov, 2014. **13**(8): p. 622-38.
- 31 28 13. Lam, J.K., et al., *siRNA Versus miRNA as Therapeutics for Gene Silencing*. Mol Ther  
32 29 *Nucleic Acids*, 2015. **4**: p. e252.
- 33 30 14. Jeric, I., et al., *A cell-autonomous tumour suppressor role of RAF1 in*  
34 31 *hepatocarcinogenesis*. Nat Commun, 2016. **7**: p. 13781.
- 35 32 15. Giambartolomei, S., et al., *Sustained activation of the Raf/MEK/Erk pathway in response*  
36 33 *to EGF in stable cell lines expressing the Hepatitis C Virus (HCV) core protein*. Oncogene,  
37 34 2001. **20**(20): p. 2606-10.
- 38 35 16. Wang, Z., et al., *Grb2-associated binder-1 plays a central role in the hepatocyte growth*  
39 36 *factor enhancement of hepatoma growth inhibition by K vitamin analog compound 5*.  
40 37 *Hepatology*, 2007. **46**(6): p. 2003-13.
- 41 38 17. Yang, S. and G. Liu, *Targeting the Ras/Raf/MEK/ERK pathway in hepatocellular*  
42 39 *carcinoma*. Oncol Lett, 2017. **13**(3): p. 1041-1047.
- 43 40 18. Schmitz, K.J., et al., *Activation of the ERK and AKT signalling pathway predicts poor*  
44 41 *prognosis in hepatocellular carcinoma and ERK activation in cancer tissue is associated*  
45 42 *with hepatitis C virus infection*. J Hepatol, 2008. **48**(1): p. 83-90.
- 46 43 19. Laloo, B., et al., *Analysis of post-transcriptional regulations by a functional, integrated,*  
47 44 *and quantitative method*. Mol Cell Proteomics, 2009. **8**(8): p. 1777-88.

- 1 20. Maurel, M., et al., *A functional screening identifies five micrornas controlling glypican-3: role of mir-1271 down-regulation in hepatocellular carcinoma*. Hepatology, 2013. **57**(1): p. 195-204.
- 2 21. Henriet, E., et al., *Argininosuccinate synthase 1 (ASS1): A marker of unclassified hepatocellular adenoma and high bleeding risk*. Hepatology, 2017. **66**(6): p. 2016-2028.
- 3 22. Kall, L., et al., *Semi-supervised learning for peptide identification from shotgun proteomics datasets*. Nat Methods, 2007. **4**(11): p. 923-5.
- 4 23. Deutsch, E.W., et al., *The ProteomeXchange consortium in 2017: supporting the cultural change in proteomics public data deposition*. Nucleic Acids Res, 2017. **45**(D1): p. D1100-D1106.
- 5 24. Agarwal, V., et al., *Predicting effective microRNA target sites in mammalian mRNAs*. Elife, 2015. **4**.
- 6 25. Dweep, H. and N. Gretz, *miRWalk2.0: a comprehensive atlas of microRNA-target interactions*. Nat Methods, 2015. **12**(8): p. 697.
- 7 26. Hwang, Y.H., et al., *Over-expression of c-raf-1 proto-oncogene in liver cirrhosis and hepatocellular carcinoma*. Hepatol Res, 2004. **29**(2): p. 113-121.
- 8 27. Boyault, S., et al., *Transcriptome classification of HCC is related to gene alterations and to new therapeutic targets*. Hepatology, 2007. **45**(1): p. 42-52.
- 9 28. Indersie, E., et al., *Tracking cellular and molecular changes in a species-specific manner during experimental tumor progression in vivo*. Oncotarget, 2018. **9**(22): p. 16149-16162.
- 10 29. Chen, L., et al., *Identification and bioinformatics analysis of miRNAs associated with human muscle invasive bladder cancer*. Mol Med Rep, 2017. **16**(6): p. 8709-8720.
- 11 30. Hironaka-Mitsuhashi, A., et al., *A tissue microRNA signature that predicts the prognosis of breast cancer in young women*. PLoS One, 2017. **12**(11): p. e0187638.
- 12 31. Wu, X., et al., *Identification and validation of potential biomarkers for the detection of dysregulated microRNA by qPCR in patients with colorectal adenocarcinoma*. PLoS One, 2015. **10**(3): p. e0120024.
- 13 32. Zhang, Q., et al., *Domain-specific c-Myc ubiquitylation controls c-Myc transcriptional and apoptotic activity*. Proc Natl Acad Sci U S A, 2013. **110**(3): p. 978-83.
- 14 33. Czubaty, A. and A. Piekuelko-Witkowska, *Protein kinases that phosphorylate splicing factors: Roles in cancer development, progression and possible therapeutic options*. Int J Biochem Cell Biol, 2017. **91**(Pt B): p. 102-115.
- 15 34. Shen, J., et al., *Epigenetic silencing of miR-490-3p reactivates the chromatin remodeler SMARCD1 to promote Helicobacter pylori-induced gastric carcinogenesis*. Cancer Res, 2015. **75**(4): p. 754-65.
- 16 35. Inoue, C., et al., *SMARCD1 regulates senescence-associated lipid accumulation in hepatocytes*. NPJ Aging Mech Dis, 2017. **3**: p. 11.
- 17 36. Hooks, K.B., et al., *New insights into diagnosis and therapeutic options for proliferative hepatoblastoma*. Hepatology, 2017.
- 18 37. Leicht, D.T., et al., *MEK-1 activates C-Raf through a Ras-independent mechanism*. Biochim Biophys Acta, 2013. **1833**(5): p. 976-86.
- 19 38. Karoulia, Z., E. Gavathiotis, and P.I. Poulidakos, *New perspectives for targeting RAF kinase in human cancer*. Nat Rev Cancer, 2017. **17**(11): p. 676-691.

- 1  
2  
3 1 39. Wang, F., et al., *miR-195 is a key regulator of Raf1 in thyroid cancer*. *Onco Targets Ther*,  
4 2 2015. **8**: p. 3021-8.  
5 3 40. Liu, Z., et al., *MiR-7-5p is frequently downregulated in glioblastoma microvasculature*  
6 4 *and inhibits vascular endothelial cell proliferation by targeting RAF1*. *Tumour Biol*,  
7 5 2014. **35**(10): p. 10177-84.  
8 6 41. Chen, L., et al., *Expression and prognostic role of pan-Ras, Raf-1, pMEK1 and pERK1/2*  
9 7 *in patients with hepatocellular carcinoma*. *Eur J Surg Oncol*, 2011. **37**(6): p. 513-20.  
10 8  
11 9  
12  
13  
14  
15  
16  
17  
18  
19  
20  
21  
22  
23  
24  
25  
26  
27  
28  
29  
30  
31  
32  
33  
34  
35  
36  
37  
38  
39  
40  
41  
42  
43  
44  
45  
46  
47  
48  
49  
50  
51  
52  
53  
54  
55  
56  
57  
58  
59  
60

Accepted version

## 1 **Figure legends**

### 2 **FIG. 1. Identification of new targets of miR-4510 by proteomics.**

3 Total proteins were extracted from Huh7 cells 24 hours after transfection with miR-4510 or a  
4 CTRL, separated, digested, and analyzed by mass spectrometry. (a) Volcano plot shows  $-\log_{10} P$   
5 value ( $y$  axis) versus fold change ( $x$  axis) of all analyzed proteins. Data were selected at a cutoff  
6 value of adjusted- $P < 0.05$ . Overall protein analysis reported 322 down-regulated (Down), 289 up-  
7 regulated (Up) and 2,688 unchanged proteins. Inset: Venn diagram shows overlaps between  
8 down-regulated proteins (DR) and target predictions using TargetScan version 7.1 or miRWalk  
9 version 3.0 algorithm. (b) Gene ontology analysis for the most significant hindered pathways upon  
10 miR-4510 versus CTRL transfections in Huh7 cells. These pathways were identified by using  
11 Ingenuity Pathway Analysis program ( $P$  value was calculated by Fisher's exact test). (c)  
12 Assessment of proteomic data by western blot. Expressions of four different proteins were  
13 analyzed following transfection of Huh7 cells. Lanes 1, 2, 3, and 4 illustrate expression levels of  
14 CDK6, SKP2, CCNB1, and RAF1 proteins, respectively, and their down-regulation upon transfection  
15 with miR-4510 as compared to CTRL. Immunodetections were quantified using ImageJ and  
16 normalized to GAPDH signal. One representative blot is shown for each protein of interest. Bars  
17 represent means  $\pm$  SD from four independent experiments in Huh7 cells (Mann-Whitney test,  $*P$   
18  $< 0.05$ ). Abbreviations: CCNB1, cyclin B1; CDK6, cyclin-dependent kinase 6; CTRL, small RNA  
19 control; GAPDH, glyceraldehyde 3-phosphate dehydrogenase; miR-4510, mature microRNA 4510;  
20 RAF1, RAF proto-oncogene serine/threonine-protein kinase; SD, standard deviation; SKP2, S-  
21 phase kinase-associated protein 2.

1  
2  
3 **1 FIG. 2. RAF1 protein is increased in a majority of HCC and inversely correlates with miR-4510 in**  
4  
5  
6 **2 biological samples.**

7  
8  
9 3 (a-b) Relative expression of RAF1 protein measured by western blotting in 27 paired T and NTL  
10  
11 4 HCC samples (see raw data in Supporting Fig. S1). (a) Horizontal lines and whiskers in scatter dot-  
12  
13 5 plot represent mean  $\pm$  SD (Wilcoxon matched-pairs signed ranked test; \*\*\* $P < 0.001$ ). (b) Results  
14  
15 6 are presented as HCC/NTL expression ratios and show a distribution of samples into three  
16  
17 7 different populations: increased, unchanged, and decreased expression of RAF1 protein in HCC  
18  
19 8 compared to NTL. The median is shown as a full line, and the reference ratio value "1" is shown  
20  
21 9 as a dotted line. Decreased subgroup includes samples with an HCC/NTL ratio  $< 0.5$ . Unchanged  
22  
23 10 subgroup includes samples with HCC/NTL ratios between 0.5 and 1.5, and increased subgroup  
24  
25 11 includes samples with an HCC/NTL ratio  $> 1.5$ . (c) Representative immunostainings of RAF1 protein  
26  
27 12 in two paired T and NTL HCC samples. The brown-stained cells in the cytoplasm and the nucleus  
28  
29 13 were considered positive for RAF1 staining. The expression of RAF1 was higher in T as compared  
30  
31 14 to NTL for both patients (scale bars = 100  $\mu\text{m}$ ). (d) Relative expression of *RAF1* mRNA in 112 HCC  
32  
33 15 and 21 NTL samples (ANOVA  $P < 0.0001$ ; Dunnett's multiple comparisons post-test; \* $P < 0.05$ , \*\* $P$   
34  
35 16  $< 0.01$ ). Expression in HCC subgroups was as indicated in the main text. (e) Inverse correlation  
36  
37 17 between RAF1 protein expression measured by western blot and miR-4510 expression measured  
38  
39 18 by RT-PCR in 17 paired T and NTL HCC samples (Spearman  $r$  correlation =  $-0.4426$ ; \* $P < 0.05$ ).  
40  
41 19 Abbreviations: ANOVA, analysis of variance; GAPDH, glyceraldehyde 3-phosphate  
42  
43 20 dehydrogenase; HCC, hepatocellular carcinoma; miR-4510, mature microRNA 4510; mRNA,  
44  
45 21 messenger RNA; NTL, nontumoral liver; RAF1, RAF proto-oncogene serine/threonine-protein  
46  
47 22 kinase; RT-PCR, real-time polymerase chain reaction; SD, standard deviation; T, tumor.

1 **FIG. 3. miR-4510 inactivates RAS/RAF/MEK/ERK pathway by directly targeting *RAF1*.**

2 (a-d) Huh7 cells were transfected with miR-4510, siRAF1, or CTRL for 72 hours. Next,  
3 RAS/RAF/MEK/ERK pathway was stimulated with EGF (0.2 ng/ $\mu$ L) for 10 minutes prior to total  
4 protein or RNA extraction. (a-c) Relative expressions of RAF1 protein (a, lane 1); pERK1/2  
5 (pERK1/2) (a, lane 2,); total ERK1/2 (a, lane 3); and two downstream effectors of  
6 RAS/RAF/MEK/ERK pathway, (b) c-FOS and (c) c-MYC, were measured by western blot.  
7 Immunosignals were quantified using ImageJ and normalized on Sypro Ruby staining of the (a)  
8 membrane or on (b-c) GAPDH signal. The migration positions of molecular weight standards (in  
9 kDa) are indicated on the sides. One representative immunoblot is shown for each experiment.  
10 Bars represent means  $\pm$  SD (n = 3; ANOVA <0.01; Dunnett's multiple comparisons post-test; \**P* <  
11 0.05, \*\**P* < 0.01, \*\*\**P* < 0.001). (d) Expression level of *RAF1* mRNA relative to  $\beta$ -*Actin* mRNA  
12 (calculated as  $2^{-\Delta\Delta C_t}$ ) was assessed by RT-PCR 72 hours after transfection with miR-4510, siRAF1,  
13 or CTRL. Bars represent mean  $\pm$  SD (n = 3; ANOVA <0.001; Dunnett's multiple comparisons post-  
14 test; \*\*\**P* < 0.001). (e) Schematic representation of *RAF1* 3'-UTR:miR-4510 duplex based on  
15 TargetScan prediction with miR-4510 site at position 219-225. Arrows indicate two point  
16 mutations (r.221C>G and r.223C>G) in *RAF1* 3'-UTR. Huh7 cells expressing GFP transgene either  
17 bearing WT or MUT *RAF1* 3'-UTR were transfected with miR-4510 or CTRL. The MFI ratio was  
18 measured using the FunREG method as indicated in the main text. Bars represent means  $\pm$  SD (n  
19 = 4; ANOVA <0.001; Bonferroni's multiple comparisons post-test; \*\**P* < 0.01). Abbreviations:  
20 ANOVA, analysis of variance; CTRL, small RNA control; ERK, extracellular signal-regulated kinase;  
21 EGF, epidermal growth factor; GFP, green fluorescent protein; MFI, mean fluorescence intensity;  
22 miR-4510, mature microRNA 4510; mRNA, messenger RNA; MUT, mutated; pERK1/2, phospho-

1 ERK1/2; RAF1, RAF proto-oncogene serine/threonine-protein kinase; RT-PCR, real-time  
2 polymerase chain reaction; SD, standard deviation; siRAF1, small interfering RNA against RAF1;  
3 UTR, untranslated region; WT, wild-type.

4  
5 **FIG. 4. RAF1 silencing impairs the tumoral behavior of HCC cells *in vitro*.**

6 (a-c) Huh7 (left panels) and Hep3B (right panels) cells were transfected with CTRL, miR-4510, or  
7 siRAF1, and the following experiments were performed: (a) Cellular growth was examined 6 days  
8 after transfection. (b) Distribution of cell cycle (percentages of cells in G<sub>0</sub>/G<sub>1</sub>, S, and G<sub>2</sub>/M phases)  
9 was analyzed 72 hours after transfection. (c) Senescent cells were quantified 8 days after  
10 transfection. (d) Huh7 cells transfected with CTRL, miR-4510, or siRAF1 were grown to confluence,  
11 and a wound was created using WoundMaker. Thus, cells were imaged with IncuCyte system  
12 every 2 hours for 24 hours (only the 24-hour end point is shown). (a-d) Bars represent means ±  
13 SD (n = 3; ANOVA <0.01; Dunnett's multiple comparisons post-test; \*P < 0.05, \*\*P < 0.01, \*\*\*P <  
14 0.001, #P = 0.0609). (e) Huh7 (top panel) and Hep3B (bottom panel) cells stably expressing the  
15 human *RAF1* transgene lacking its 5'- and 3'-UTRs (RAF1) or an empty transgene (Empty) were  
16 established by lentiviral transduction. Stable expressing cells were further transfected with CTRL  
17 or miR-4510, and cellular growth was measured every 24 hours for 6 days using IncuCyte system.  
18 Data are plotted as the percentage of confluence versus time ± SD (n = 3; 2-way ANOVA <0.001;  
19 Tuckey's multiple comparisons post-test; Empty/CTRL versus RAF1/CTRL: \*\*P < 0.01, \*\*\*P <  
20 0.001; Empty/CTRL versus Empty/miR-4510 at 144hr: ###P < 0.001; RAF1/CTRL versus RAF1/miR-  
21 4510 at 144 hours: \$\$\$P < 0.001; Empty/miR-4510 versus RAF1/miR-4510: &P < 0.05, &&P < 0.01,

1 &&& $P < 0.001$ ). Abbreviations: ANOVA, analysis of variance; CTRL, small RNA control; HCC,  
2 hepatocellular carcinoma; miR-4510, mature microRNA 4510; mRNA, messenger RNA; RAF1, RAF  
3 proto-oncogene serine/threonine-protein kinase; SD, standard deviation; siRAF1, small  
4 interfering RNA against RAF1; UTR, untranslated region.

5  
6 **FIG. 5. RAF1 silencing inhibits HCC tumor development *in vivo*.**

7 (a) Timeline illustrating the CAM assay. Twenty-four hours after transfection with miR-4510 or  
8 CTRL, Huh7 cells were collected and grafted on the CAM at day 10 of embryonic development (= day 0 of tumor age). Thus, tumor growth was monitored from day 11 to day 16 by  
9 stereomicroscopy. Tumors aged of 6 days were extracted and fixed in formalin. (b) Lanes 1 and 2:  
10 representative pictures of tumor having grown on CAM (top panels, scale bars = 3 mm) and after  
11 extraction and formalin-fixation (lane 2 panels, scale bars = 3 mm) at day 16. Lane 3:  
12 representative pictures of 6-day-aged tumors stained by HES (middle panels, scale bars = 100  $\mu\text{m}$ ).  
13 Lanes 4 and 5: representative pictures of RAF1 (lane 4 panels) and Ki67 (bottom panels)  
14 immunostainings in 6-day-aged tumors (scale bars = 50  $\mu\text{m}$ ). Magnifications were as indicated. (c-  
15 d) On day 6 after miR-4510- or CTRL-transfected Huh7 cell implantation, (c) extracted tumor mass  
16 was weighed, and (d) tumor thickness was measured with ImageJ using formalin-fixed paraffin-  
17 embedded tissue sections. The total number of eggs analyzed per group is indicated in brackets  
18 above the corresponding condition. Horizontal line and whiskers represent mean  $\pm$  SD (Mann-  
19 Whitney test; \*\*\* $P < 0.001$ ). (e) Representative pictures of RAF1 immunostaining in tumors  
20 deriving from Huh7 cells transfected with miR-4510 or CTRL (scale bars = 50  $\mu\text{m}$ ). (b and e, lanes  
21

1  
2  
3 1 4 and 5) The brown-stained cells were considered positive either for RAF1 or Ki67 protein.  
4

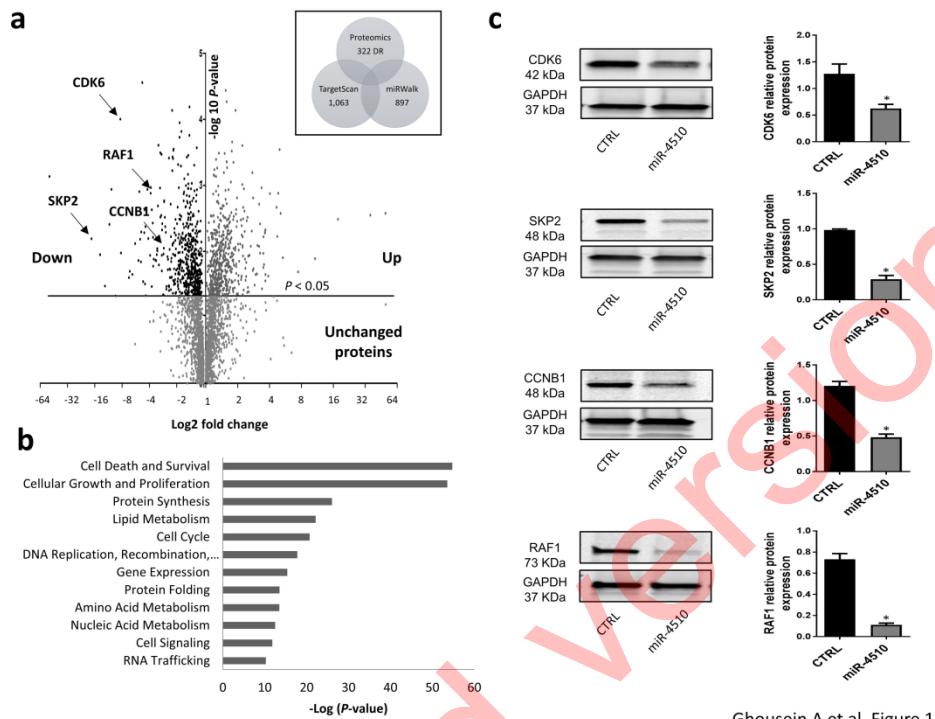
5 2 Abbreviations: CAM, chick chorioallantoic membrane; CTRL, small RNA control; HCC,  
6  
7  
8 3 hepatocellular carcinoma; HES, hematoxylin eosin saffron; miR-4510, mature microRNA 4510;  
9  
10 4 mRNA, messenger RNA; RAF1, RAF proto-oncogene serine/threonine-protein kinase; SD,  
11  
12  
13 5 standard deviation.  
14  
15

16 6  
17  
18  
19  
20  
21  
22  
23  
24  
25  
26  
27  
28  
29  
30  
31  
32  
33  
34  
35  
36  
37  
38  
39  
40  
41  
42  
43  
44  
45  
46  
47  
48  
49  
50  
51  
52  
53  
54  
55  
56  
57  
58  
59  
60

Accepted version

1  
2  
3 **1 Author contributions**  
4

5 2 Amani Ghousein and Nicola Mosca performed the cellular and molecular analyses, the *in vivo*  
6  
7 3 analyses, and the histological staining. Justine Charpentier assisted in performing the cellular analyses.  
8  
9 4 Flora Cartier prepared transfected cells and protein extracts for proteomic analyses. Anne-Auréli  
10  
11 5 Raymond and Jean-William Dupuy performed mass spectrometry and differential expression analysis.  
12  
13 6 Amani Ghousein, Anne-Auréli Raymond, and Christophe F. Grosset performed bioinformatic and  
14  
15 7 statistical analyses. Paulette Bioulac-Sage provided tissue samples and clinical data, obtained written  
16  
17 8 informed consent and ethical approvals, and performed histological analysis. Amani Ghousein and  
18  
19 9 Christophe F. Grosset wrote the manuscript. Christophe F. Grosset supervised the work and obtained the  
20  
21 10 grants supporting this work.  
22  
23  
24  
25  
26  
27  
28  
29  
30  
31  
32  
33  
34  
35  
36  
37  
38  
39  
40  
41  
42  
43  
44  
45  
46  
47  
48  
49  
50  
51  
52  
53  
54  
55  
56  
57  
58  
59  
60

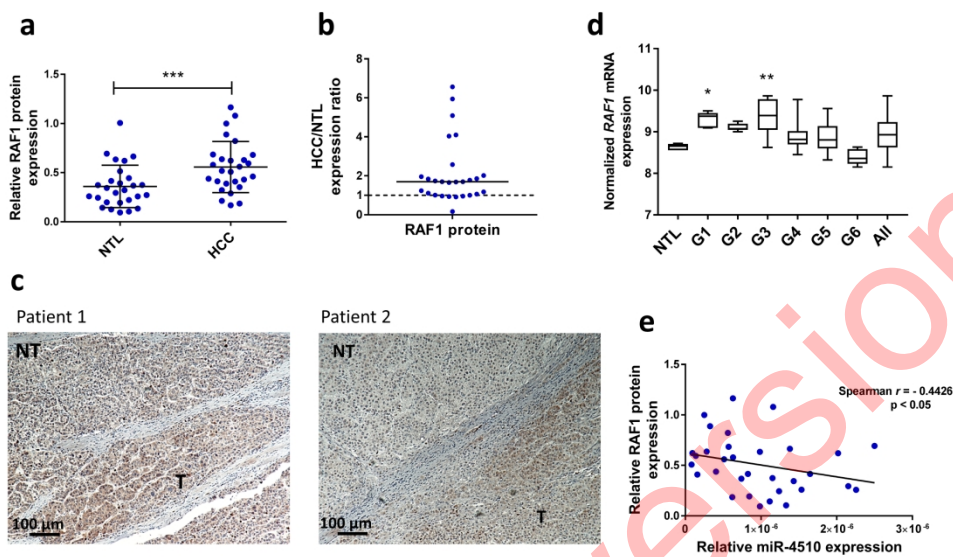


Ghoussein A et al, Figure 1

Figure 1

254x190mm (300 x 300 DPI)

Accepted Version



Ghousein A et al, Figure 2

Figure 2

254x190mm (300 x 300 DPI)

Accepted Version

1  
2  
3  
4  
5  
6  
7  
8  
9  
10  
11  
12  
13  
14  
15  
16  
17  
18  
19  
20  
21  
22  
23  
24  
25  
26  
27  
28  
29  
30  
31  
32  
33  
34  
35  
36  
37  
38  
39  
40  
41  
42  
43  
44  
45  
46  
47  
48  
49  
50  
51  
52  
53  
54  
55  
56  
57  
58  
59  
60

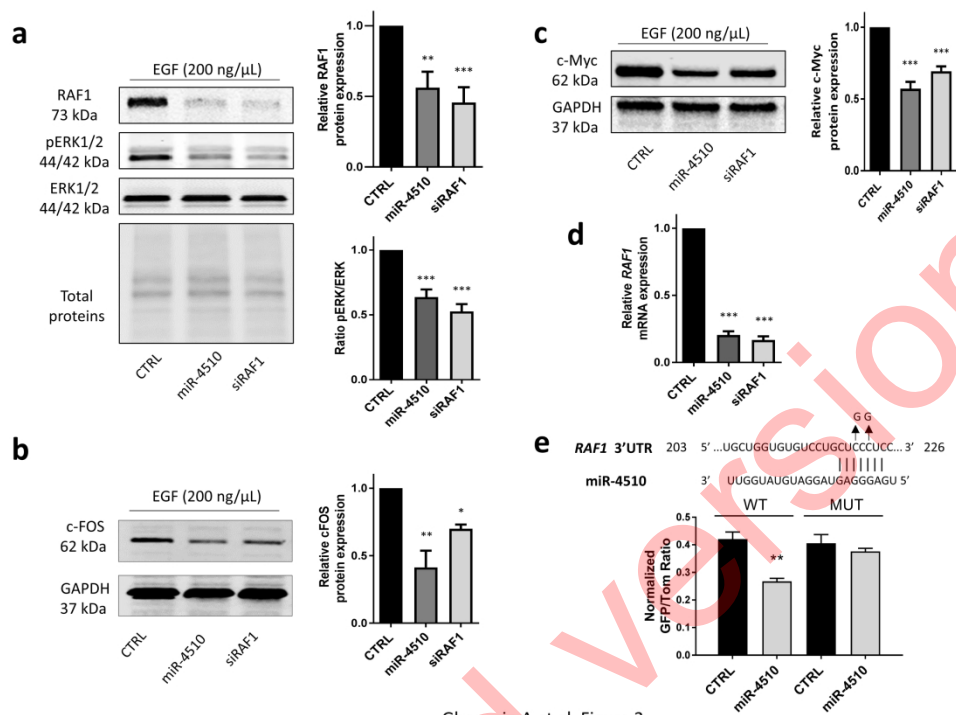
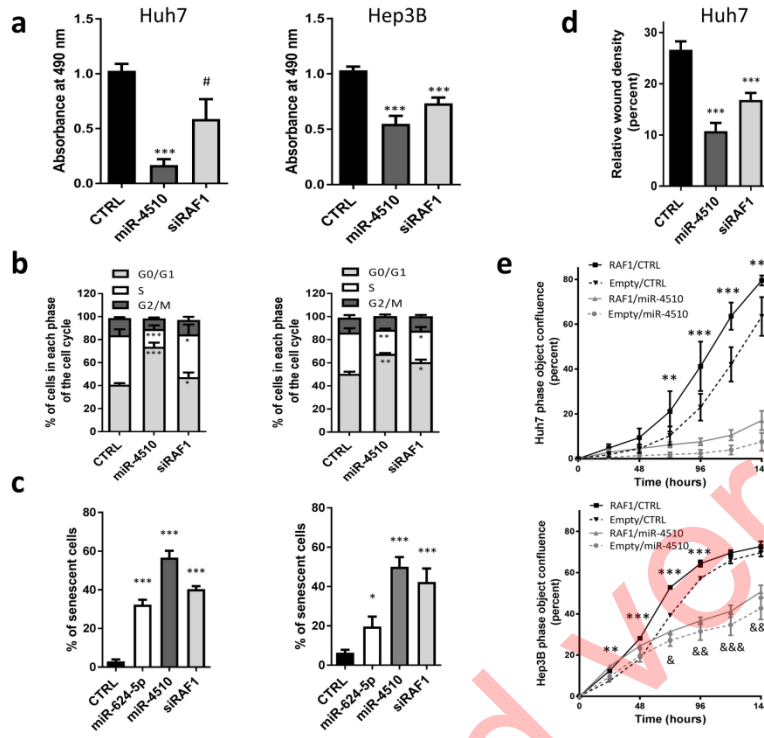


Figure 3

254x190mm (300 x 300 DPI)



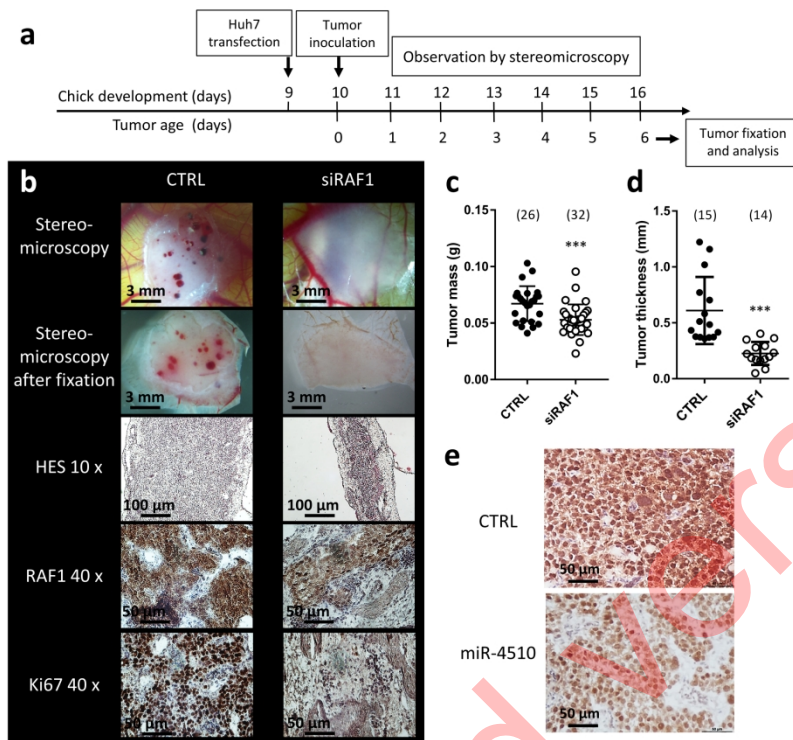
Ghoussein A et al, Figure 4

Figure 4

254x190mm (300 x 300 DPI)

Accepted Manuscript

1  
2  
3  
4  
5  
6  
7  
8  
9  
10  
11  
12  
13  
14  
15  
16  
17  
18  
19  
20  
21  
22  
23  
24  
25  
26  
27  
28  
29  
30  
31  
32  
33  
34  
35  
36  
37  
38  
39  
40  
41  
42  
43  
44  
45  
46  
47  
48  
49  
50  
51  
52  
53  
54  
55  
56  
57  
58  
59  
60



Ghosein A et al, Figure 5

Figure 5

254x190mm (300 x 300 DPI)

Accepted Article

## Supplementary Material

### Plasmid constructions

The lentiviral vectors pL-GFP-3'UTR-RAF1-WT and pL-GFP-3'UTR-RAF1-MUT were designed by inserting either the synthetic wild-type (WT) or mutated (MUT) (mutations r.221C>G and r.223C>G) *RAF-1* 3'-untranslated region (UTR) in the BsrGI site-digested pL-GFP plasmid.<sup>[1]</sup> The NM-002880.3 sequence was used as a backbone for the sequencing of *RAF1* 3'-UTR into the pEX-A2 insert-donor plasmid (Eurofins Genomics, Germany).

For the pL-RAF1 vector, the open reading frame (ORF) of RAF1 was amplified from pLX304 vector (ORF ccsbBroad304\_06837, Dharmacon, Inc., Lafayette, CO) using the forward primer GCGGATCCACCATGGAGCACATACAGGGAGC (underlined nucleotides represent the BamHI restriction site) and the reverse primer GCGCTAGCTTAGTAGACAGGCAGCCTCGG (underlined nucleotides represent the NheI restriction site). The obtained polymerase chain reaction (PCR) product was subcloned into an intermediary TA vector (TA Cloning Kit, Invitrogen, Carlsbad, CA, USA). Next, the obtained plasmid was cut with BamHI and NheI, and the insert containing RAF1 ORF was purified. In parallel, pL-GFP was cut with the same restriction enzymes to remove Green Fluorescent Protein (GFP) coding region where RAF1 ORF was ligated instead, thus yielding the pL-RAF1 vector that was used to produce infectious lentiviral particles.

### RNA isolation and quantitative real-time PCR

Total RNA was extracted from cultured cells using Trizol (Sigma, St Louis, MO, USA) reagent or mirVana miRNA Isolation Kit (Life Technologies, Carlsbad, CA, USA) according to the manufacturer's instructions. miR-4510 expression was measured as described previously [2]. To quantify mRNA expression, complementary DNA was synthesized with the Maxima Reverse Transcriptase kit (Thermo Scientific, Waltham, MA, USA). Quantitative PCR (qPCR) amplifications were performed in 12- $\mu$ L multiplex PCR reactions containing 1X SYBR Green Supermix (Quanta Biosciences, Beverly, MA, USA)

on a C1000 Thermal Cycler (Bio-Rad, Hercules, CA, USA). Beta-actin was used as internal control. The relative mRNA levels of gene expression were calculated using the  $2^{-\Delta\Delta Ct}$  method. The primer sequences were RAF1 forward (5' GGAGACACATGGGATTTTGG 3') and reverse (5' GCTGTGAAAGGAGGACGTGT 3') and beta-actin forward (5' TCCCTGGAGAAGAGCTACGA 3') and reverse (5' AGCACTGTGTTGGCGTACAG 3'), all purchased from Eurofin Genomics. Primer efficiency was between 95% and 105%. miR-4510 expression was measured as described before [2].

### **Cell viability assay**

A total of 3,000 cells/well were seeded in 96-well plates, and cell proliferation was evaluated by using tetrazolium compound-based CellTiter 96 AQueous One Solution Cell Proliferation (3-(4,5-dimethylthiazol-2-yl)-5-(3-carboxymethoxyphenyl)-2-(4-sulfophenyl)-2H-tetrazolium [MTS]) assay (Promega, Madison, WI, USA), according to the manufacturer's instructions. Then, 20  $\mu$ L of the MTS reagent solution was added to each well and incubated at 37°C in 5% CO<sub>2</sub> for 2 hours. Cell proliferation was assessed at days 1 and 6 after transfection. Absorbance was read at 490 nm using a ClarioStar (BMG Labtech, Ortenberg, Allemagne).

### **Cell cycle**

Cell cycle analysis was performed using the APC BrdU flow kit (BD Pharmingen, San Diego, CA) according to the manufacturer's instructions. Briefly, 200,000 cells were seeded into a 6-well plate with volume 2 mL and then transfected. After 3 days, BrdU was added into the cell culture medium for 45 minutes. The incorporated BrdU was detected using an APC anti-BrdU fluorescent antibody, and the levels of cell-associated BrdU were measured by flow cytometry using a fluorescence-activated cell sorting (FACS) CANTO II (BD Biosciences, San Jose, CA, USA).

### **Cell death assays**

Prior to apoptosis detection, 200,000 cells were seeded into a 6-well plate in a volume of 2 mL and transfected. Three days later, total cells were collected, and apoptosis was analyzed using the Annexin V-PE/7-Amino-Actinomycin (AAD) apoptosis detection kit (BD Pharmingen, San Diego, CA). Viable cells with intact membranes exclude 7-ADD and are PE Annexin V negative. Fluorescence generated by the cell-bound Annexin V-PE, which measures the percentage of early apoptotic cells, and the 7AAD, which measures the percentage of late apoptotic cells, were analyzed by FACS. Total apoptosis was calculated by adding the percentage of late apoptotic cells (Annexin V-PE<sup>High</sup>/7ADD<sup>High</sup>) and the percentage of early apoptotic cells (Annexin V-PE<sup>High</sup>/7ADD<sup>Low</sup>).

### **Cell senescence assay**

Cell senescence was assessed using the Senescence Beta-Galactosidase Staining kit (Cell Signaling, Danvers, MA, USA) according to manufacturer's instructions. Cells were plated in a 24-well plate at a density of 5,000 cells/well in a volume of 500  $\mu$ L and transfected by either CTRL, miR-4510, siRAF1, or miR-624-5p. After 4 days, cells were trypsinized and seeded onto a cover slip 24-well plate where they were subjected to second transfection. Four days later, cells were fixed, and beta-galactosidase activity was revealed by the addition of X-gal and staining solution. Cells were counterstained by eosin 0.5% and observed under a microscope. Only blue cells were counted as a measure of senescence.

### **Wound healing and migration assays**

Huh7 cells were transfected with miR-4510, siRAF1, or CTRL. After 24 hours, cells were trypsinized and moved into 96-well plates where they were seeded at a density of 15,000 cells. Six hours later, a wound

was created using WoundMaker, and cells were imaged with IncuCyte (Essen BioSciences, USA) every 2 hours for 24 hours. To obtain more homogeneous layers of Huh7 cells, especially after transfection with the pro-apoptotic and pro-senescent miR-4510, two-well cell culture inserts (Biovalley, France) were used. Huh7 cells were transfected with miR-4510 or CTRL. After 48 hours, cells were trypsinized and moved into 2-well culture inserts at a density of 50,000 cells per well. Eighteen hours later, empty-space colonization by cells was imaged at 8, 24 and 48 hours with an InCellis microscope (Bertin Technologies, France) and quantifications were performed with Image J.

### **FunREG and DF-FunREG screening**

FunREG and DF-FunREG analyses were performed 3 days after transfection as described [1, 3] with minor modifications, including fluorescence measurements using CLARIOstar multiplate reader (BMG Labtech, Ortenberg, Allemagne).

### **Immunohistochemistry**

The 3.5- $\mu$ m-thick sections were de-paraffinized and rehydrated, and antigen retrieval was performed in a citrate buffer pH 9 solution. All staining procedures were performed by an autostainer (Dako-Agilent Clara, USA) using standard reagents provided by the manufacturer. The sections were incubated with rabbit anti-RAF-1 (1:250, ab154754, Abcam) or mouse anti-Ki67 (1:100, M7240, Dako). Incubation in horseradish peroxidase (EnVision Flex/HRP, Dako-Agilent) or secondary AB for 20 minutes was used for signal amplification. 3,3'-diamino-benzidine (DAB, Dako) development was used for detecting primary antibodies. The slides were counterstained with hematoxylin, dehydrated, and mounted. Each immunohistochemical run contained a negative control (buffer, no primary antibody). Sections were visualized with a Nikon-Eclipse501 microscope, and images were acquired using NIS-Elements F.

## References

1. Maurel, M., et al., *A functional screening identifies five micrornas controlling glypican-3: role of mir-1271 down-regulation in hepatocellular carcinoma*. *Hepatology*, 2013. **57**(1): p. 195-204.
2. Cartier, F., et al., *New tumor suppressor microRNAs target glypican-3 in human liver cancer*. *Oncotarget*, 2017. **8**(25): p. 41211-41226.
3. Indersie, E., et al., *MicroRNA therapy inhibits hepatoblastoma growth in vivo by targeting beta-catenin and Wnt signaling*. *Hepatol Commun*, 2017. **1**(2): p. 168-183.

Accepted version

## Supplementary Figures

**Supplementary FIG. S1. Expression of RAF1 protein in tumoral and nontumoral tissues from HCC patients.** Total proteins were extracted from 27 paired T and adjacent NTL HCC samples and 2 normal liver specimens from the same patient (NL1) that were used as controls. Thus, RAF1 protein level was quantified by western blotting in P samples using Huh7 cell protein extract as internal C. Immunodetections were normalized on Sypro Ruby staining of the membranes and on C. Abbreviations: C, calibrator; NL1, normal liver; NTL, nontumoral liver; P, patient; T, tumor.

**Supplementary FIG. S2. Immunostaining of RAF1 protein in tumoral and nontumoral tissues from HCC patients.** (a) HES staining of sectioned tissues (scale bars = 100  $\mu$ m). (b) RAF1 immunostaining of sectioned tissues. Pictures show difference in expression between the tumoral and nontumoral parts of the liver (scale bars = 100  $\mu$ m). (c) A normal liver tissue was sectioned at 3.5  $\mu$ m thickness. The left panel shows HES staining, and the right panel shows RAF1 immunostaining (scale bars = 100  $\mu$ m). RAF1 staining is negative in normal liver. Abbreviation: HES, hematoxylin eosin saffron.

**Supplementary FIG. S3. miR-4510 or siRAF1 inhibits RAF1 protein expression in transfected Hep3B cells.** Expression levels of RAF1 protein assessed by western blot on Hep3B whole cell extracts 72 hours after transfection with miR-4510, siRAF1, or CTRL. Immunodetections were normalized on GAPDH signal. The migration positions of molecular weight standards (in kDa) are

indicated on the sides. One representative immunoblot is shown. Bars represent means  $\pm$  SD (n = 3; ANOVA  $<0.001$ ; Dunnett's multiple comparisons post-test;  $***P < 0.001$ ). Abbreviations: ANOVA, analysis of variance; CTRL, small RNA control; HES, hematoxylin eosin saffron; SD, standard deviation; siRAF1, small interfering RNA against RAF1.

**Supplementary FIG. S4. miR-4510 or RAF1 silencing inhibits HCC cell proliferation.** (a-b)

Representative data of APC BrdU/7-AAD measurements performed by flow cytometry in (a) Huh7 cells and (b) Hep3B cells transfected with miR-4510, siRAF1, or CTRL.

**Supplementary FIG. S5. miR-4510 or RAF1 silencing induces senescence of HCC cells.** (a-b) Huh7

and Hep3B cells were transfected with the indicated small RNAs. Eight days later, cells were stained for beta-galactosidase activity and counterstained with eosin. Blue cells were considered positive. Representative pictures (scale bars = 100  $\mu$ m) of (a) X-gal-positive Huh7 and (b) Hep3B cells.

**Supplementary FIG. S6. miR-4510 induces apoptosis, but RAF1 silencing has limited pro-**

**apoptotic ability.** (a-b) Representative data of Annexin V/7AAD staining measured by flow cytometry in (a) Huh7 cells and (b) Hep3B transfected with miR-4510, siRAF1, or CTRL. For each small RNA, the left graphs represent the cell population selected to analyze apoptosis in the right graphs. Q1: early apoptotic cells; Q2: late apoptotic cells; Q3: viable cells; Q4: nonviable cells. As

shown in the top right panel, total apoptosis was calculated by adding the percentage of late apoptotic cells (Annexin V-PE<sup>High</sup>/7ADD<sup>High</sup>) and the percentage of early apoptotic cells (Annexin V-PE<sup>High</sup>/7ADD<sup>Low</sup>). Bars represent means  $\pm$  SD (n = 3; ANOVA <0.05; Dunnett's multiple comparisons post-test; \**P* < 0.05, \*\*\**P* < 0.001).

**Supplementary FIG. S7. Combined apoptotic effect of miR-4510 and Sorafenib on HCC cells. (a)**

Two days after transfection by miR-4510 or control RNA (Ctrl), Huh7 cells were treated with 10 $\mu$ M sorafenib for 24 hours. Thus, the percentage of apoptotic cells was measured (n=3, ANOVA *p*<0.001; Bonferroni's multiple comparisons test: \* *p*<0.05; \*\*\* *p*<0.001). (b-c) Treatment of Huh7 cells by 10 $\mu$ M sorafenib strongly decreased RAF1 protein expression (b) and induced miR-4510 expression. (b) Immunoblots showing RAF1 and GAPDH signals. The migration position of the proteins compared to the molecular weight standards is as indicated in kDa. Immunoblots of three independent experiments are shown. (c) Relative expression of miR-4510 in Huh7 cells treated or not by Sorafenib (Soraf). Bars represent means  $\pm$  SD (n = 6; two-tailed Wilcoxon matched-pairs signed rank test; \**P* < 0.05).

**Supplementary FIG. S8. miR-4510 or RAF1 silencing inhibits migration of Huh7 cells. (a)**

Representative picture of migrating Huh7 cells 24 hours after wound creation. Huh7 cells were transfected with the indicated small RNAs and grown to confluence. Thus, a wound was created (T = 0 hours), and the plate was placed in the IncuCyte system. Migration was monitored by taking pictures every 2 hours for 24 hours (24-hour end point is shown). (b) Left panel: Representative

picture of migrating Huh7 cells at 0, 8, 24 and 48 hours after removal of the 2-well culture insert. Right panel: Percentage of area closure using Huh7 cells transfected with Control RNA (CTRL) or miR-4510. Bars represent means  $\pm$  SD (n=3, two-way ANOVA  $p < 0.001$ ; Sidak's multiple comparisons test: \*\*\*  $p < 0.001$ ).

**Supplementary FIG. S9. Ectopic expression of RAF1 protein in Huh7 and Hep3B cells following lentiviral transduction.** Huh7 and Hep3B cells were transduced at an MOI of 5 with lentivirus either harboring the RAF1 transgene lacking its 3'- and 5'-UTRs or an empty transgene. Then, 24 hours after transduction, cells were washed and amplified. Next, total proteins were extracted from each cell line, and the expression of RAF1 protein was examined by western blot. Immunodetections were normalized on Sypro Ruby staining of the membrane. The migration positions of molecular weight standards (in kDa) are indicated on the sides. One representative immunoblot is shown. Bars represent mean  $\pm$  SD (n = 3; Mann-Whitney test; \* $P < 0.05$ ). Abbreviation: MOI, multiplicity of infection.

**Supplementary FIG. S10. Effect of miR-4510 transfection on RAF1 protein level in Huh7 cells ectopically expressing RAF1 transgene or an empty transgene.** Huh7 cells stably expressing RAF1 transgene or an empty (Empty) transgene were transfected with miR-4510 or CTRL. Then, 72 hours after transfection, cells were lysed, and total proteins were extracted. Relative level of RAF1 protein expression was quantified by western blot. Immunodetections were normalized on GAPDH signal. The migration positions of molecular weight standards (in kDa) are indicated

on the sides. One representative immunoblot is shown. Bars represent means  $\pm$  SD (n = 3; ANOVA  $<0.001$ ; Dunnett's multiple comparisons post-test; \* $P < 0.05$ , \*\*\* $P < 0.001$ ).

**Supplementary FIG. S11. RAF1 silencing impairs HCC growth *in vivo*.** (a-b) HES staining of Huh7 cell-derived tumors grown on the CAM after transfection with (a) CTRL or (b) siRAF1 (scale bars = 100  $\mu$ m). (c-d) RAF1 staining of Huh7 cell-derived tumors grown on the CAM after transfection with (c) CTRL or (d) siRAF1 (scale bars = 50  $\mu$ m). One representative blank tissue section is shown. (e-f) Ki67 staining of Huh7 cell-derived tumors grown on the CAM after transfection with (e) CTRL or (f) siRAF1 (scale bars = 50  $\mu$ m). One representative blank tissue section is shown. Brown-stained cells were considered positive.

**Supplementary FIG. S12. miR-4510 decreases RAF1 expression *in vivo*.** (a-b) HES staining of Huh7 cell-derived tumors grown on the CAM after transfection with (a) CTRL or (b) miR-4510 (scale bars = 100  $\mu$ m). (c-d) RAF1 staining of Huh7 cell-derived tumors grown on the CAM after transfection with (c) CTRL or (d) miR-4510 (scale bars = 50  $\mu$ m). One representative blank tissue section is shown. Brown-stained cells were considered positive.

**Supplementary FIG. S13. RAF1 5'-UTR contains two predicted miR-4510 sites.** Schematic representation of RAF1 untranslated regions (UTR):miR-4510 duplexes based on predictions with

RNA Hybrid for RAF1 5'-UTR and TargetScan for 3'-UTR (ref: NM\_002880.3, Homosapiens Raf-1 proto-oncogene, serine/threonine protein kinase, mRNA).

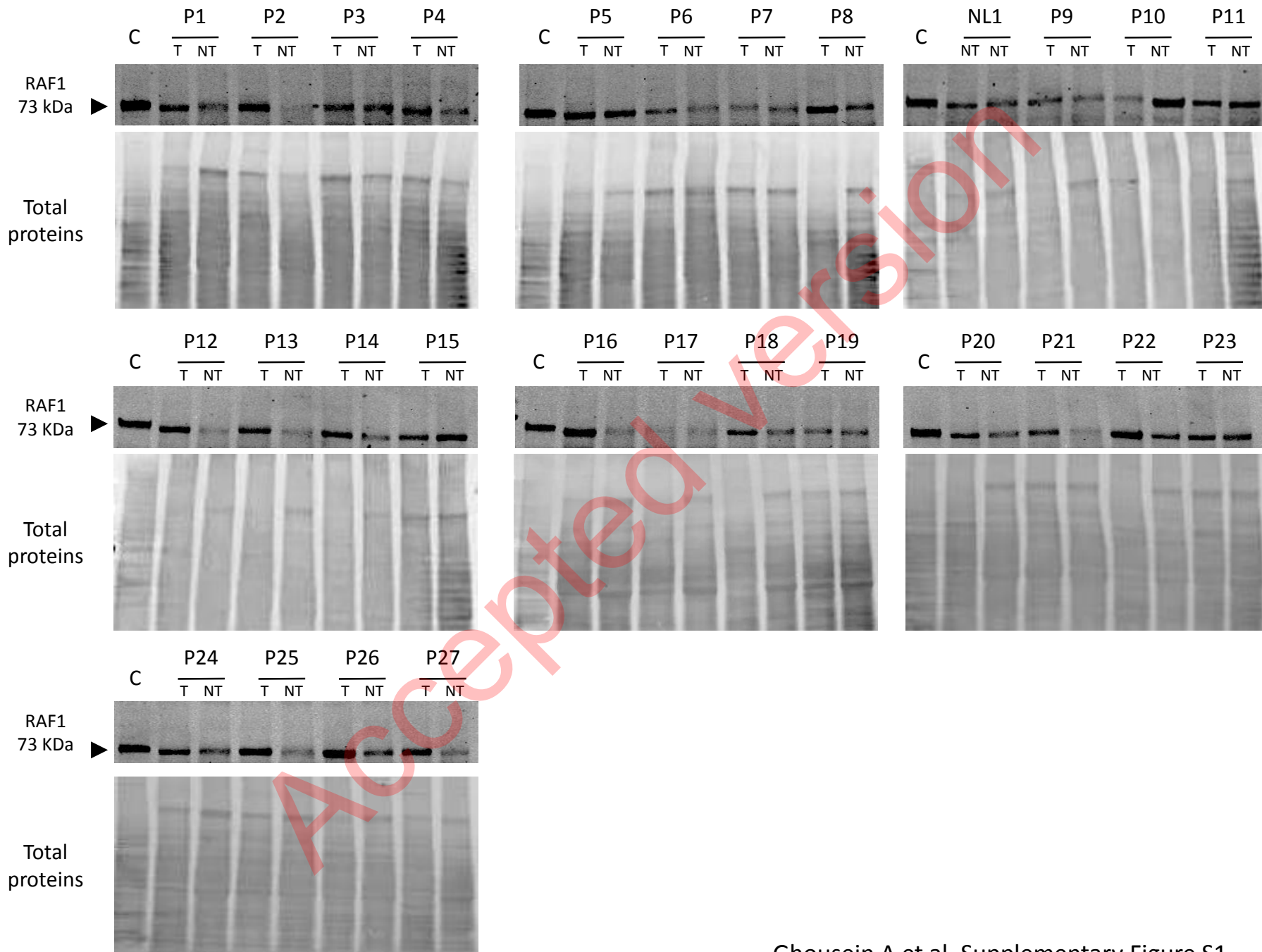
Accepted version

**Supplementary Table S1: Clinical and genetic features of 27 paired tumor and nontumoral liver HCC samples of our cohort.**

| <b>Variables</b>                           | <b>Features</b> | <b>Number of cases (%)</b> |
|--|-----------------|----------------------------|
| Gender                                     | Male/Female     | 22(81.5%)/5 (18.5%)        |
| Age  | mean (min, max) | 64.9 (39-79)               |
| Tumor differentiation<br>(Edmondson)       | II              | 5 (18.5%)                  |
|  | II/III          | 11 (40.7%)                 |
|  | III             | 7 (25.9%)                  |
|  | III/IV          | 3 (11.2%)                  |
|  | IV              | 1 (3.7%)                   |
| Etiology                                   | Alcohol         | 11 (40.7%)                 |
|  | HCV             | 10 (37%)                   |
|  | HBV             | 3 (11.2%)                  |
|  | Hemochromatosis | 0 (0%)                     |
|  | Other           | 3 (11.2%)                  |
| Fibrosis in non-tumoral liver<br>(METAVIR) | F0              | 4 (14.8%)                  |
|  | F1              | 3 (11.2%)                  |
|  | F2              | 4 (14.8%)                  |
|  | F3              | 6 (22.2%)                  |
|  | F4              | 10 (37%)                   |
| <b>CTNNB1</b>                              | Mutated         | 4 (14.8%)                  |
|  | Nonmutated      | 23 (85.2%)                 |

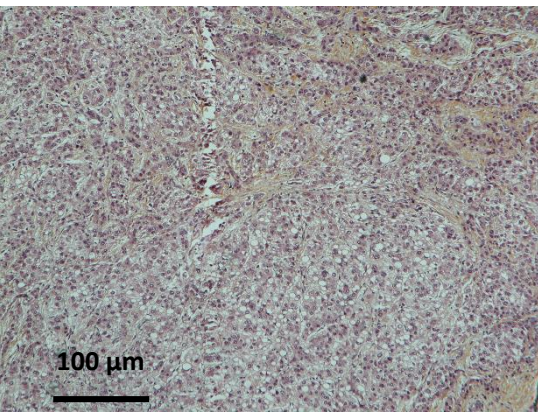
**Supplementary Table S4: Cellular and molecular processes and genes deregulated in miR-4510-transfected Huh7 cells.**

| Categories                                 | Genes   |
|--|---|
| Cellular Growth and Proliferation          | <b>RAF1</b> , COL14A1, MYH9, IGF2BP3, CCL20, SOD2         |
| Protein Synthesis                          | <b>RAF1</b> , APOB, MYH9, IGF2BP3, NCSTN, ARHGEF1         |
| Cell Cycle                                 | <b>RAF1</b> , MYH9, ANKRD17, NCAPG, SOD2, EZR             |
| DNA Replication, Recombination, and Repair | <b>RAF1</b> , MCM6, SRPK1, NCAPG, CUL4A, SART1, PBK, SOD2 |
| Gene Expression                            | <b>RAF1</b> , JAK1, CUL4A, RPS6KA3, PPP4C, SMARCA4        |

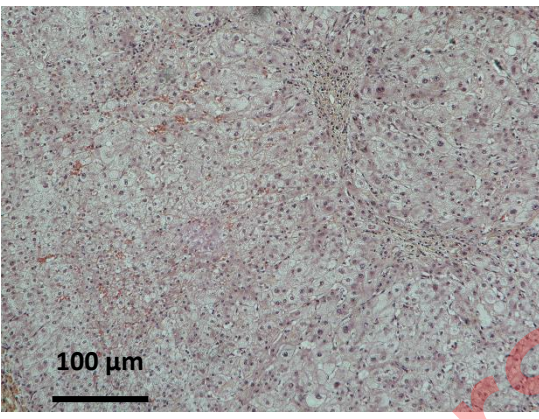


**a**

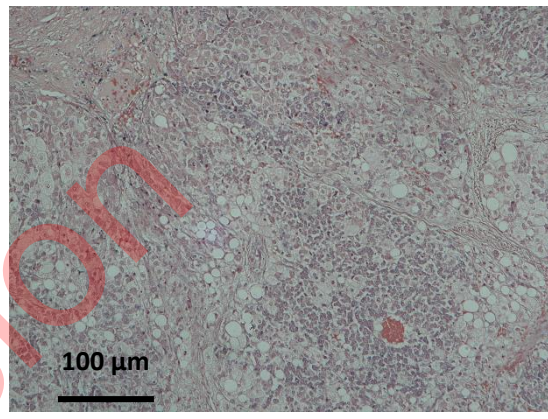
Patient 1



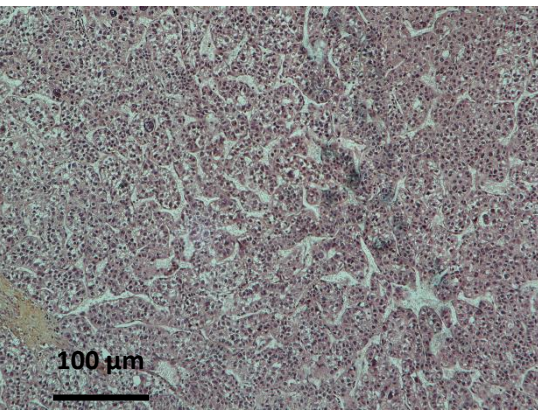
Patient 2



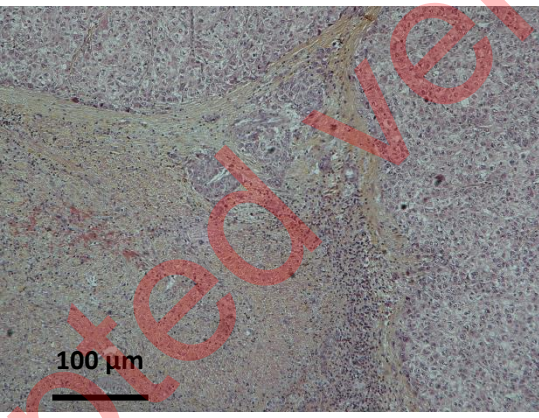
Patient 3



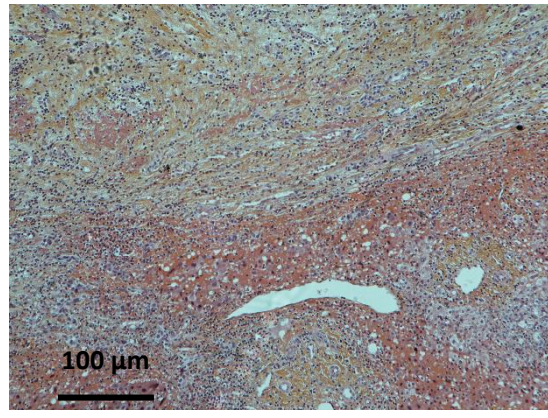
Patient 4



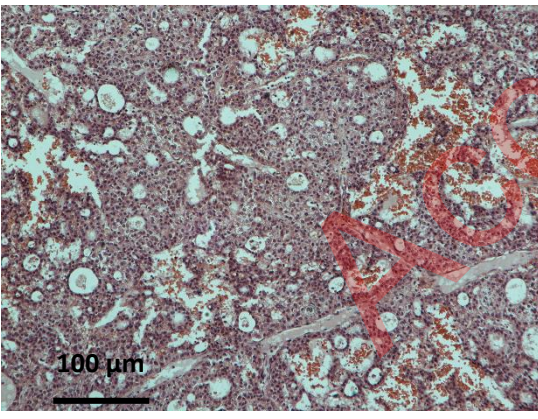
Patient 5



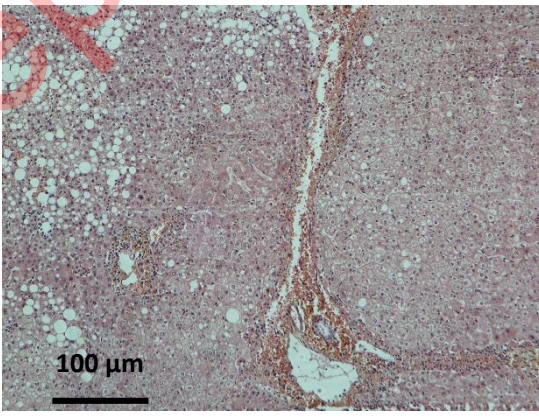
Patient 6



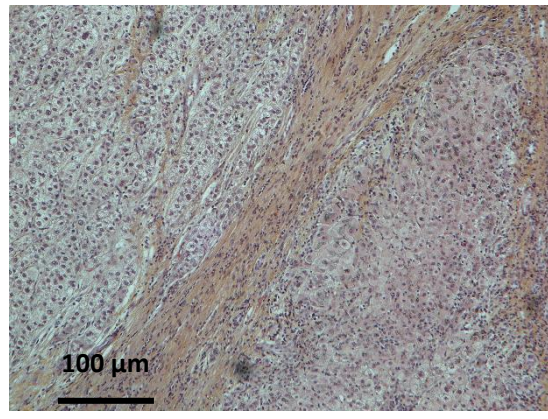
Patient 7



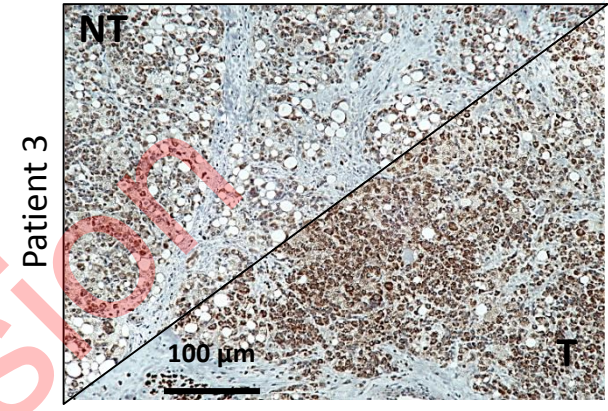
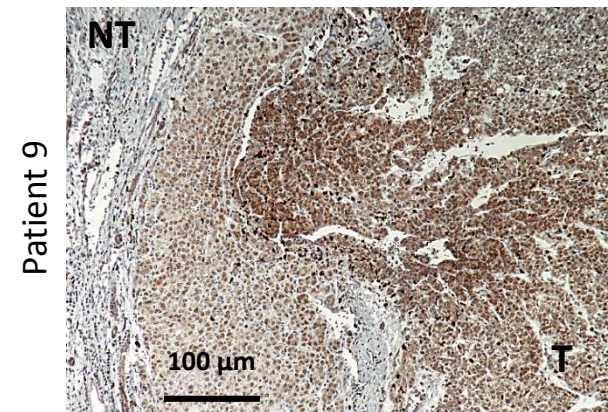
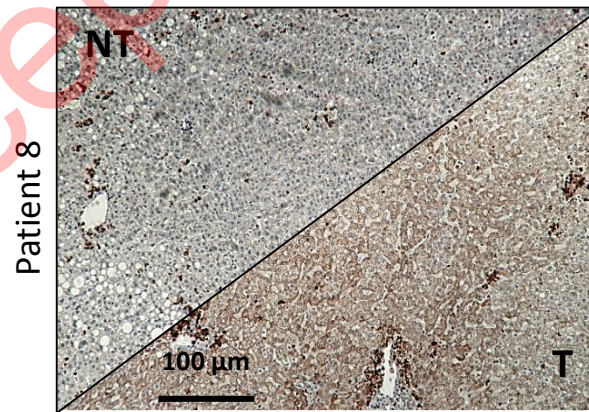
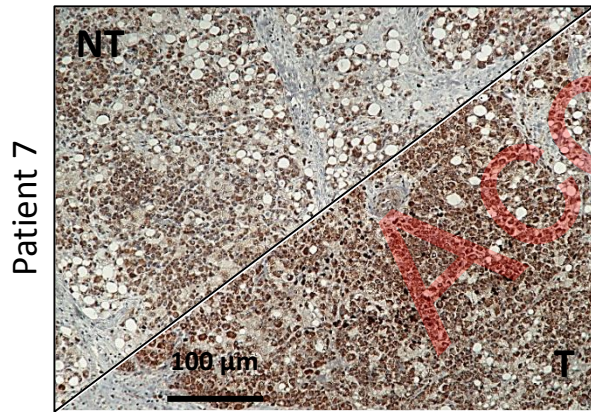
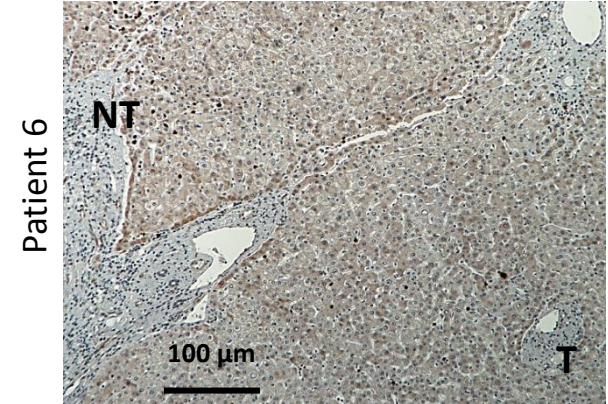
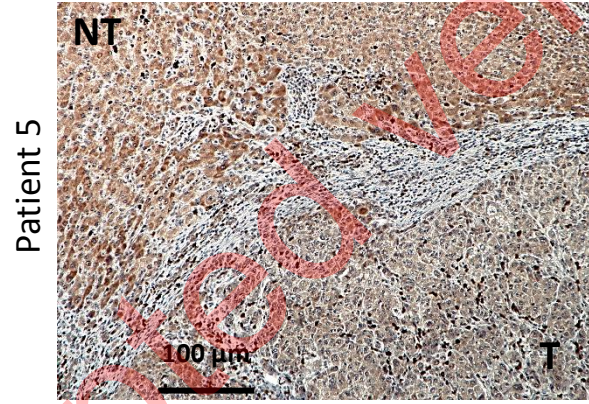
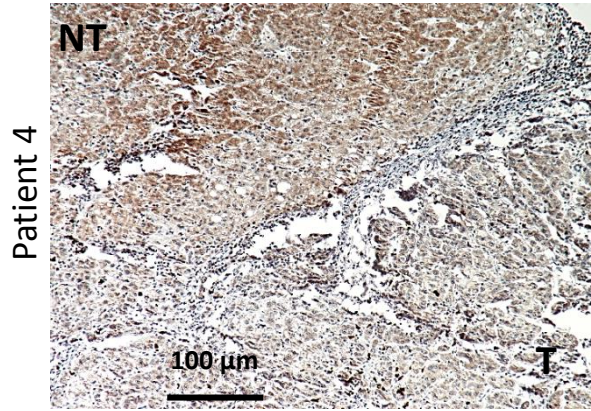
Patient 8



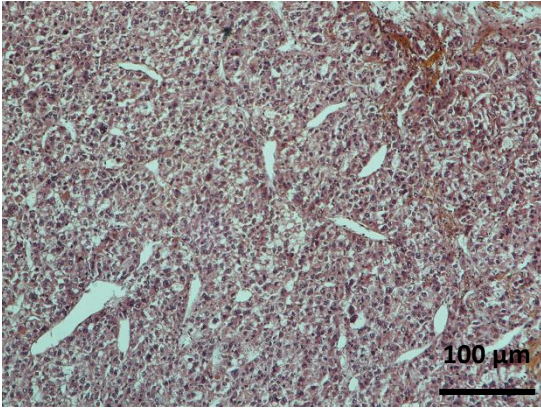
Patient 9



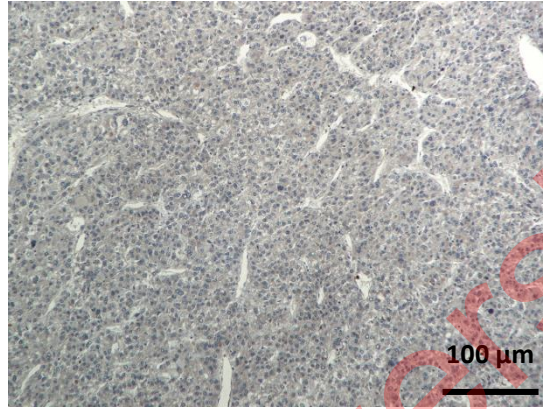
**b**



**c**



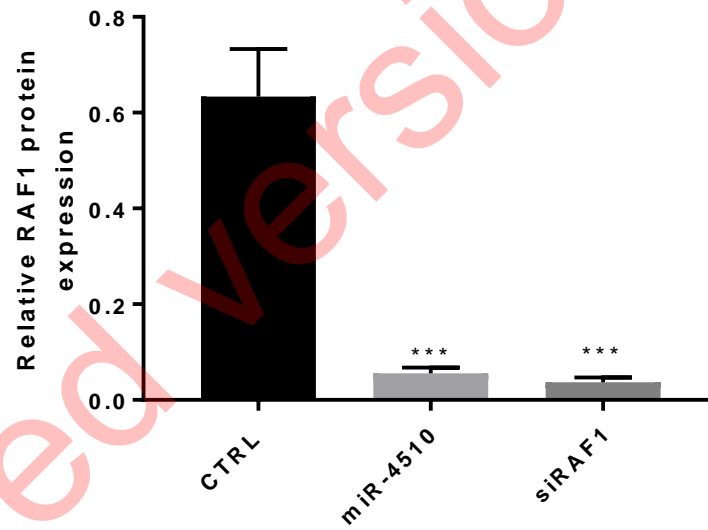
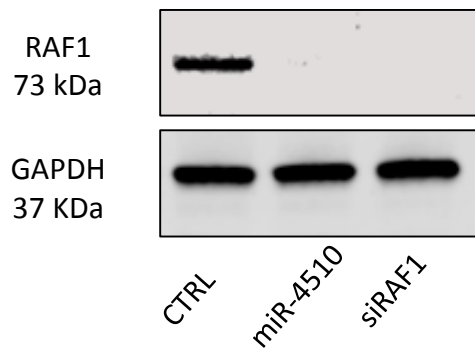
HES

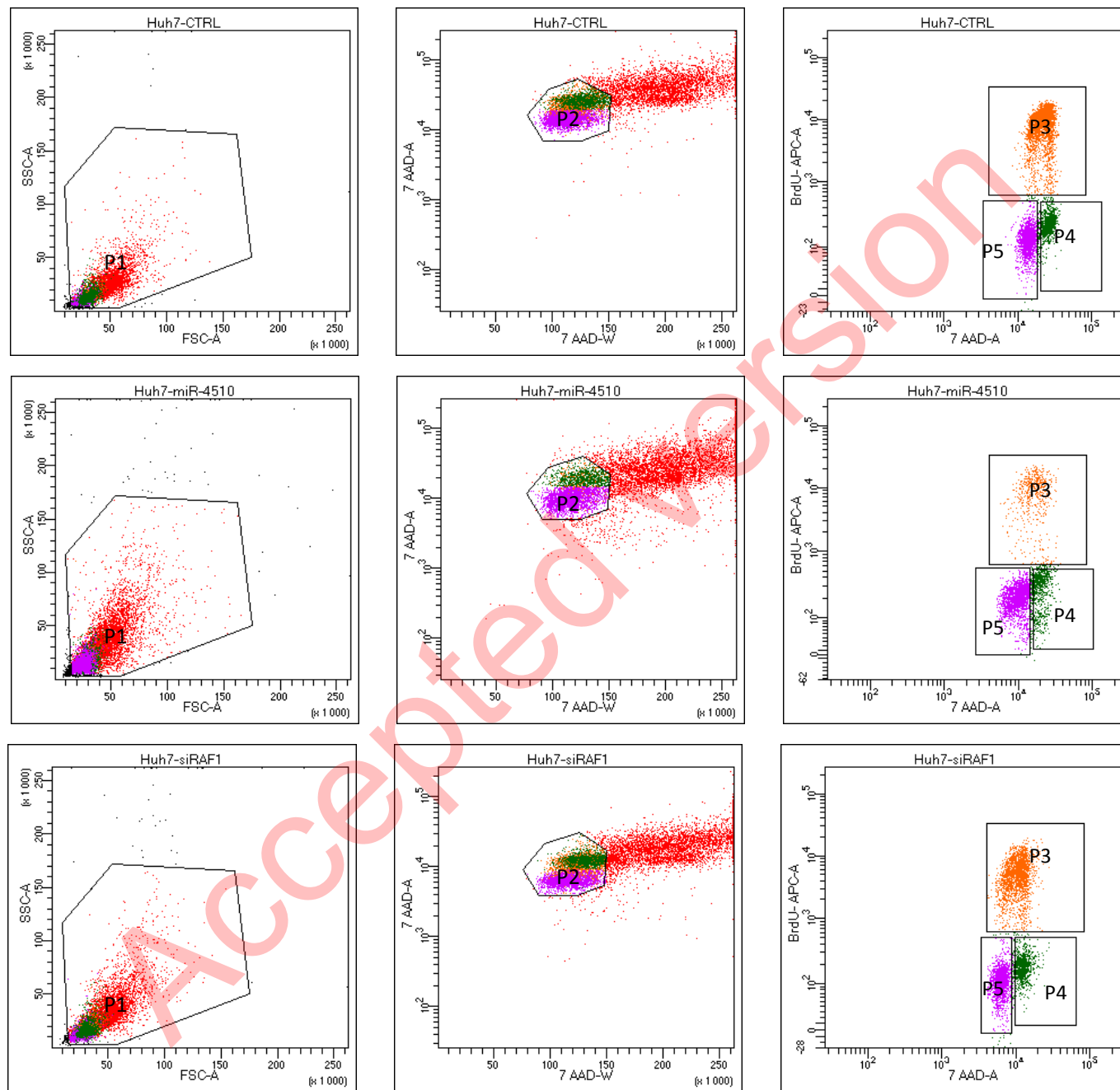


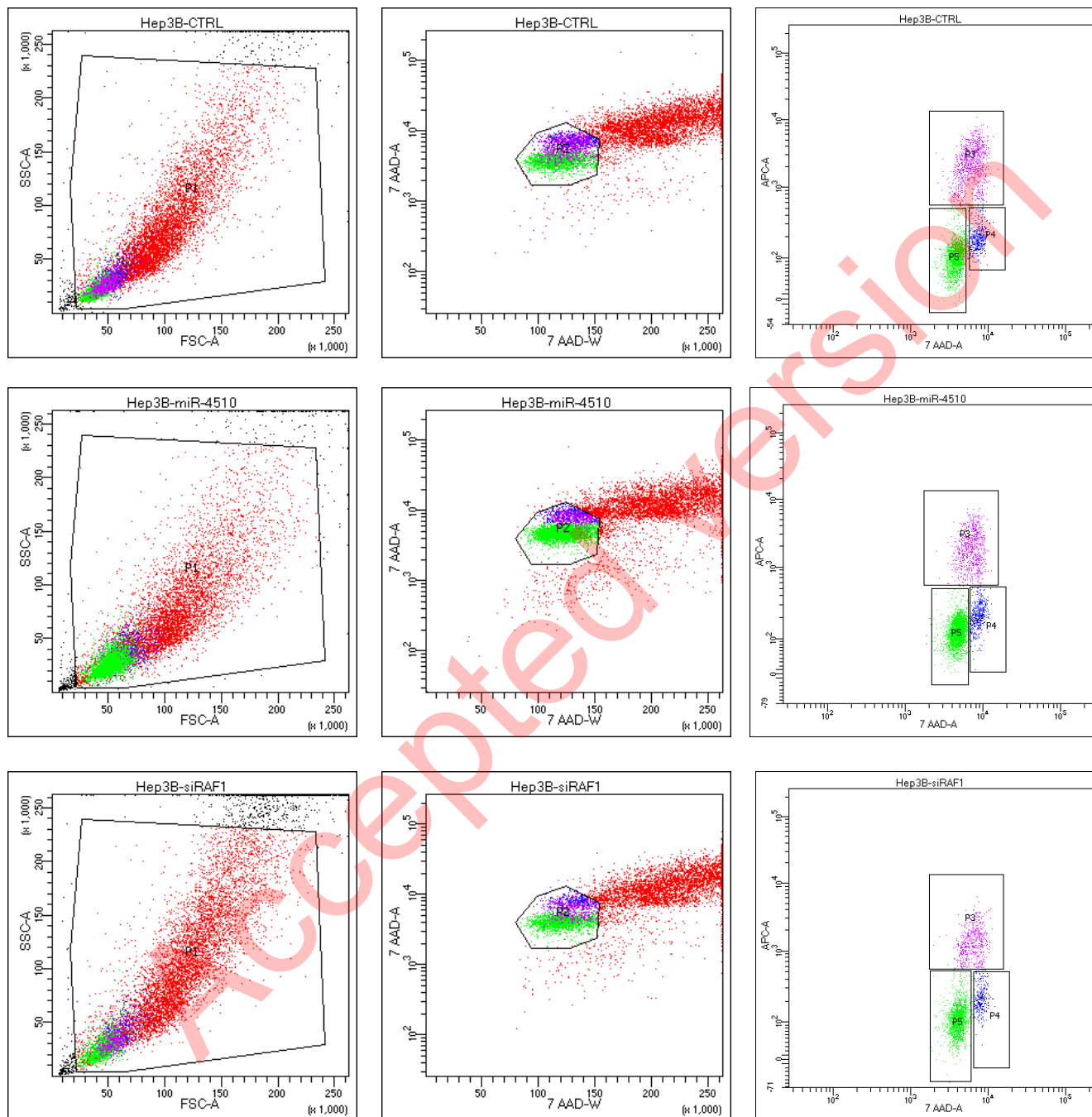
RAF1  
immunostaining

Accepted Version

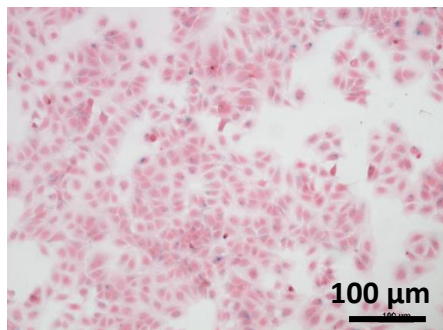
Hep3B cells



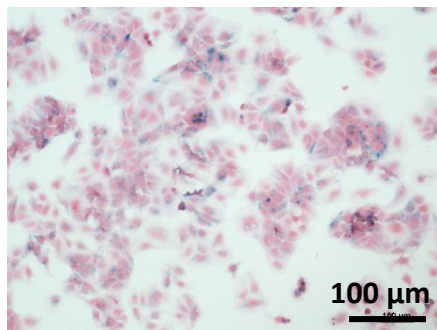
**a**

**b**

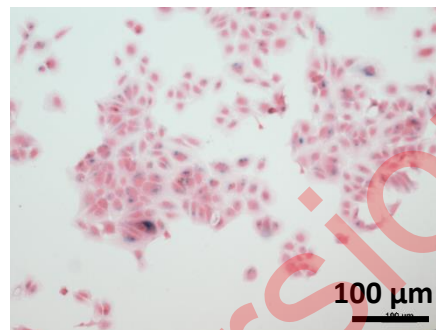
**a** Huh7 cells



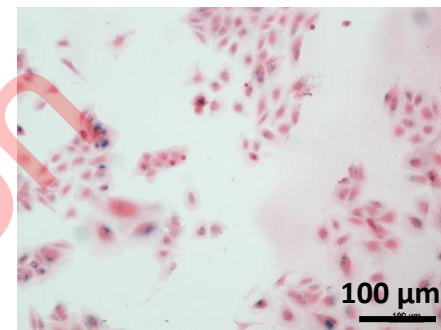
CTRL



miR-4510

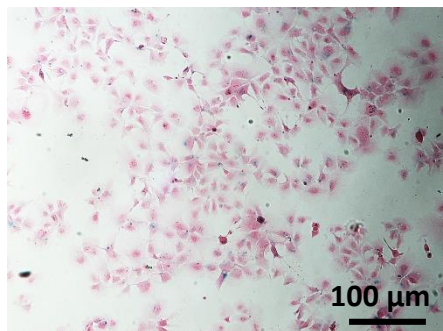


siRAF1



miR-624-5p

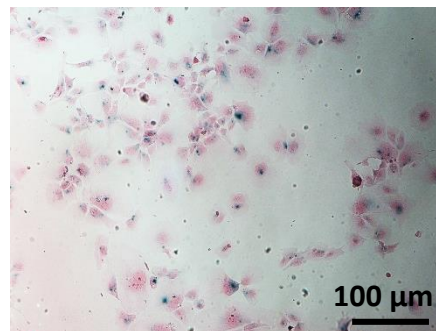
**b** Hep3B cells



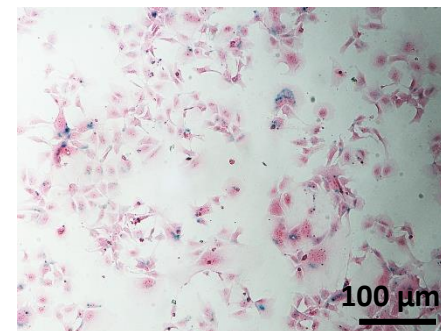
CTRL



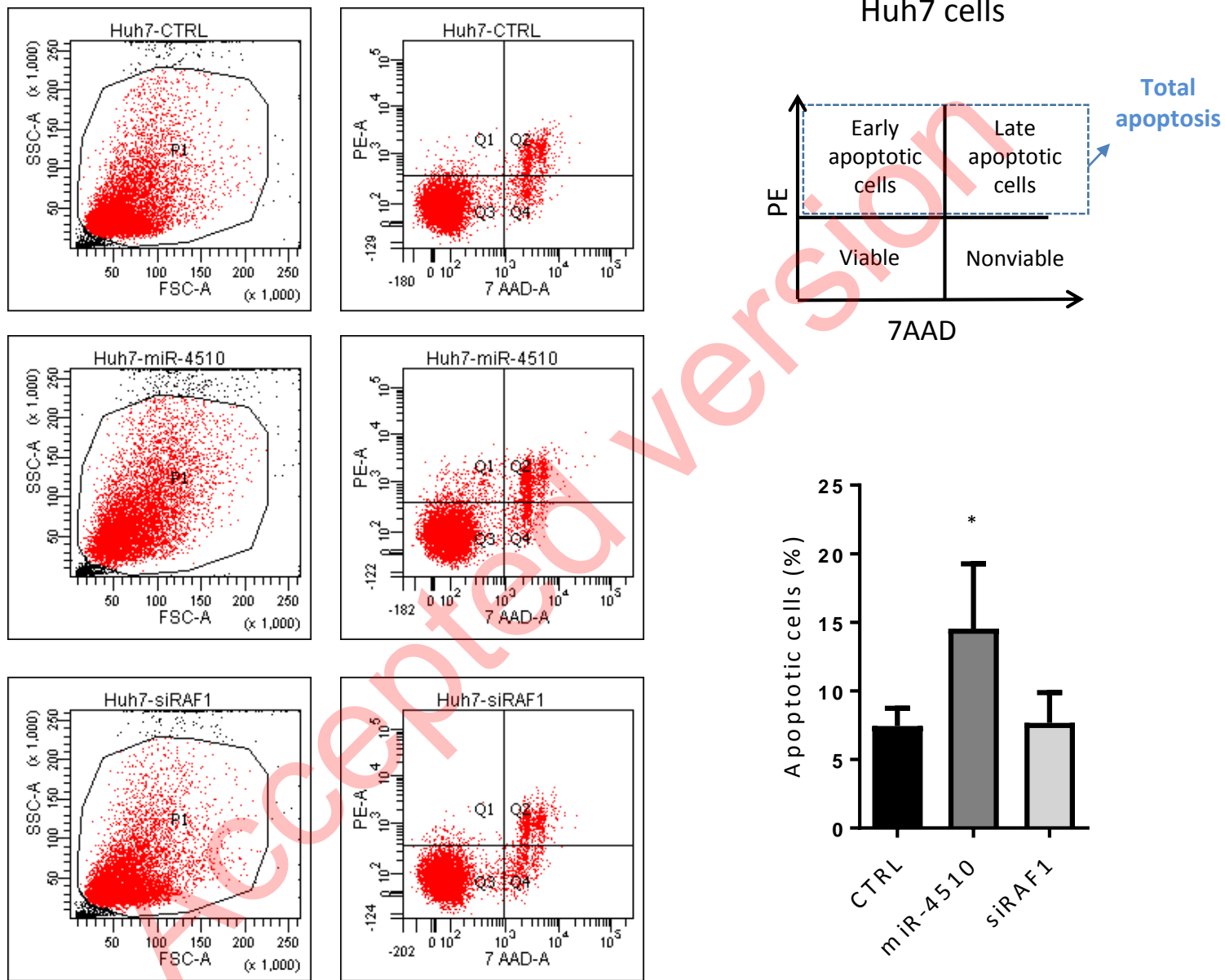
miR-4510

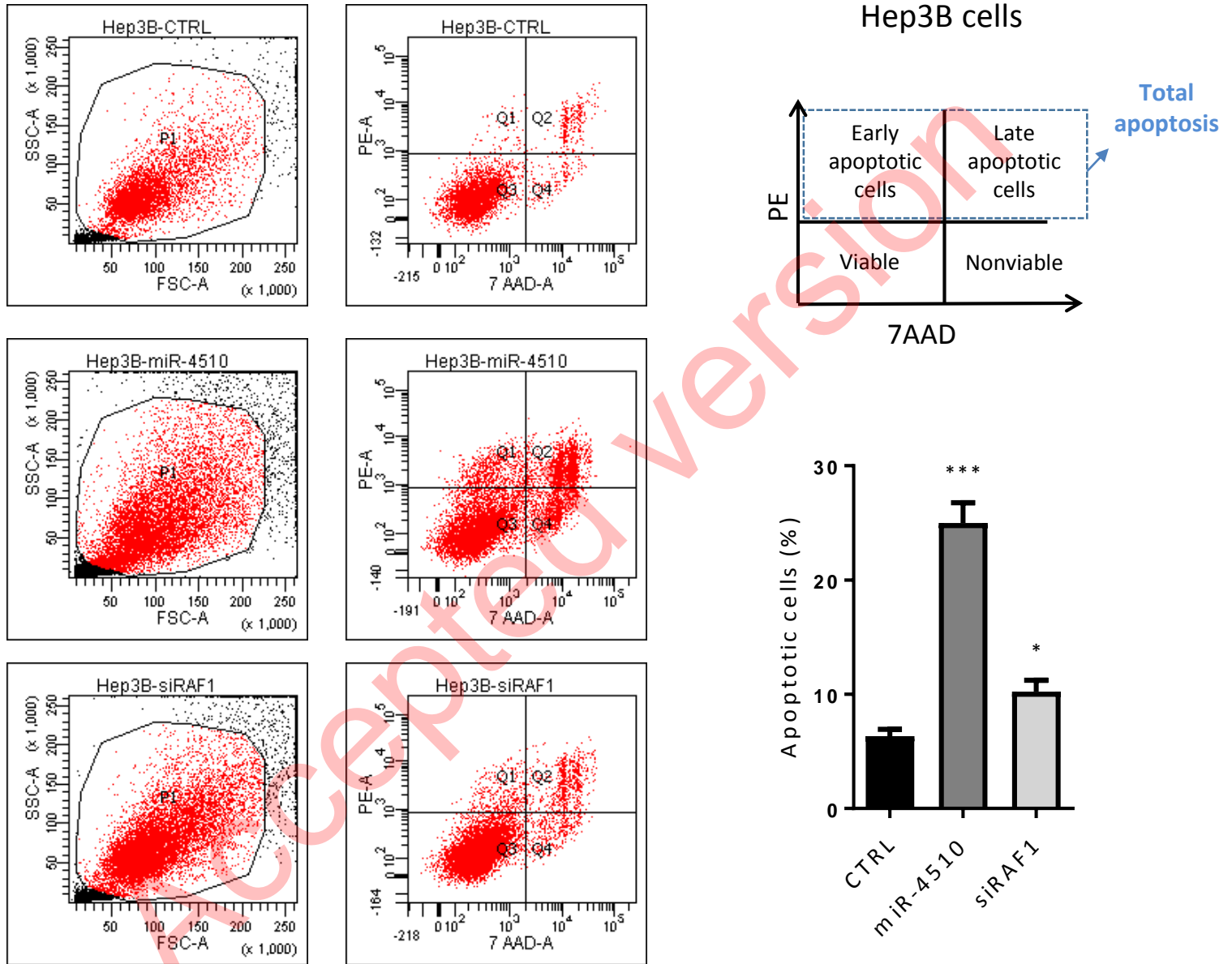


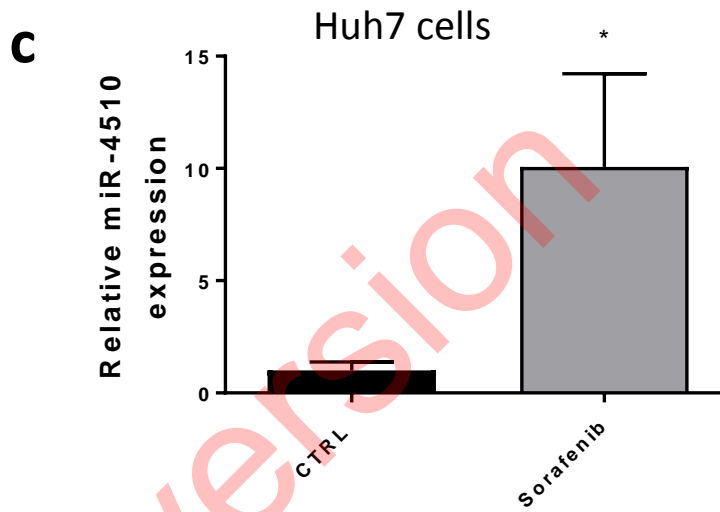
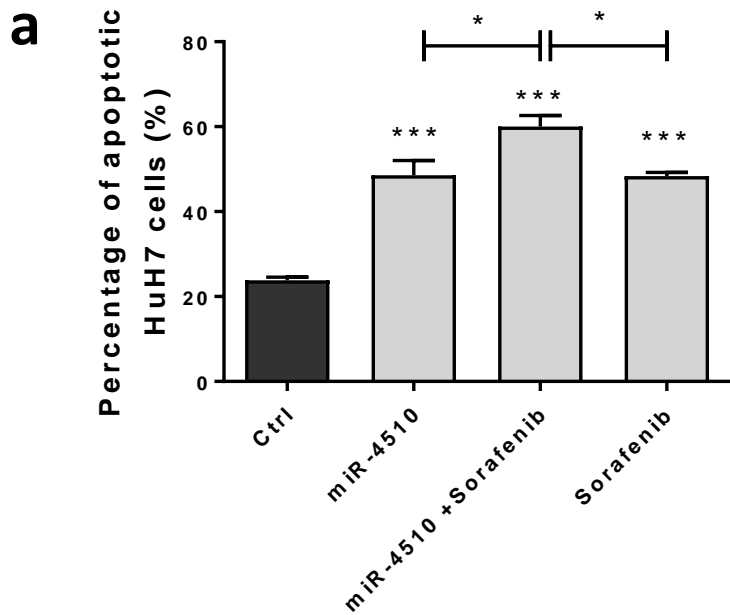
siRAF1



miR-624-5p

**a**

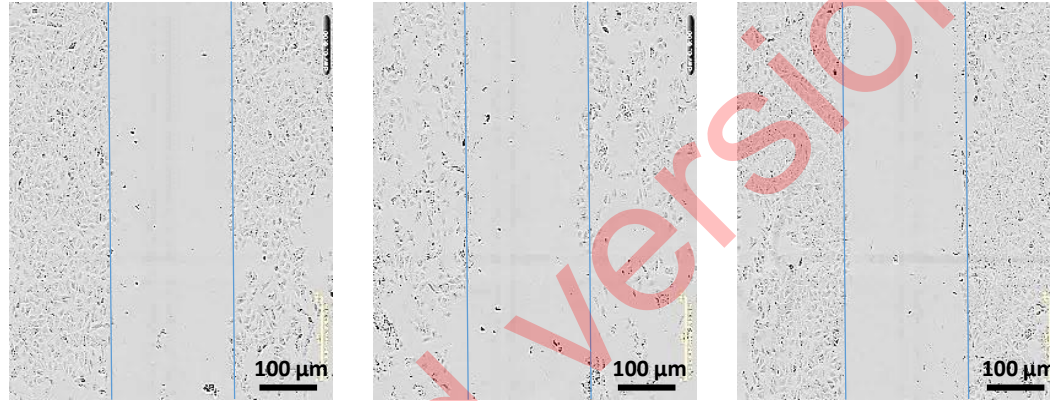
**b**



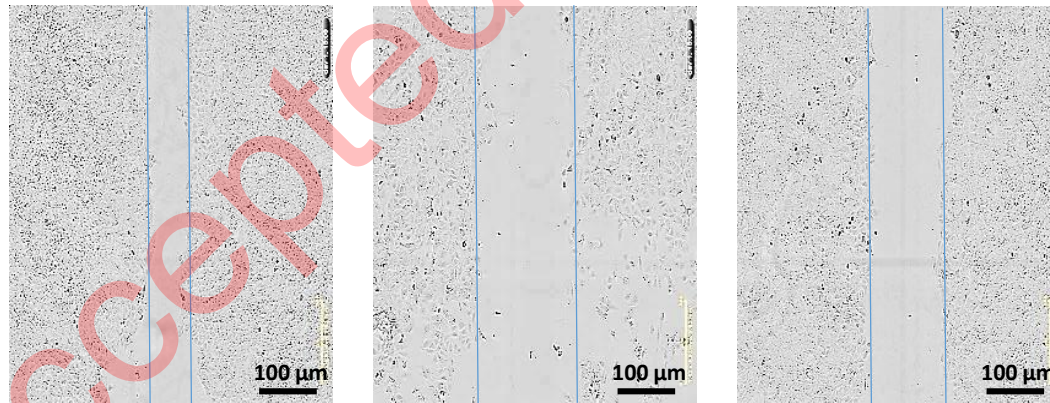
**a**

Huh7 cells

T = 0h



T = 24h



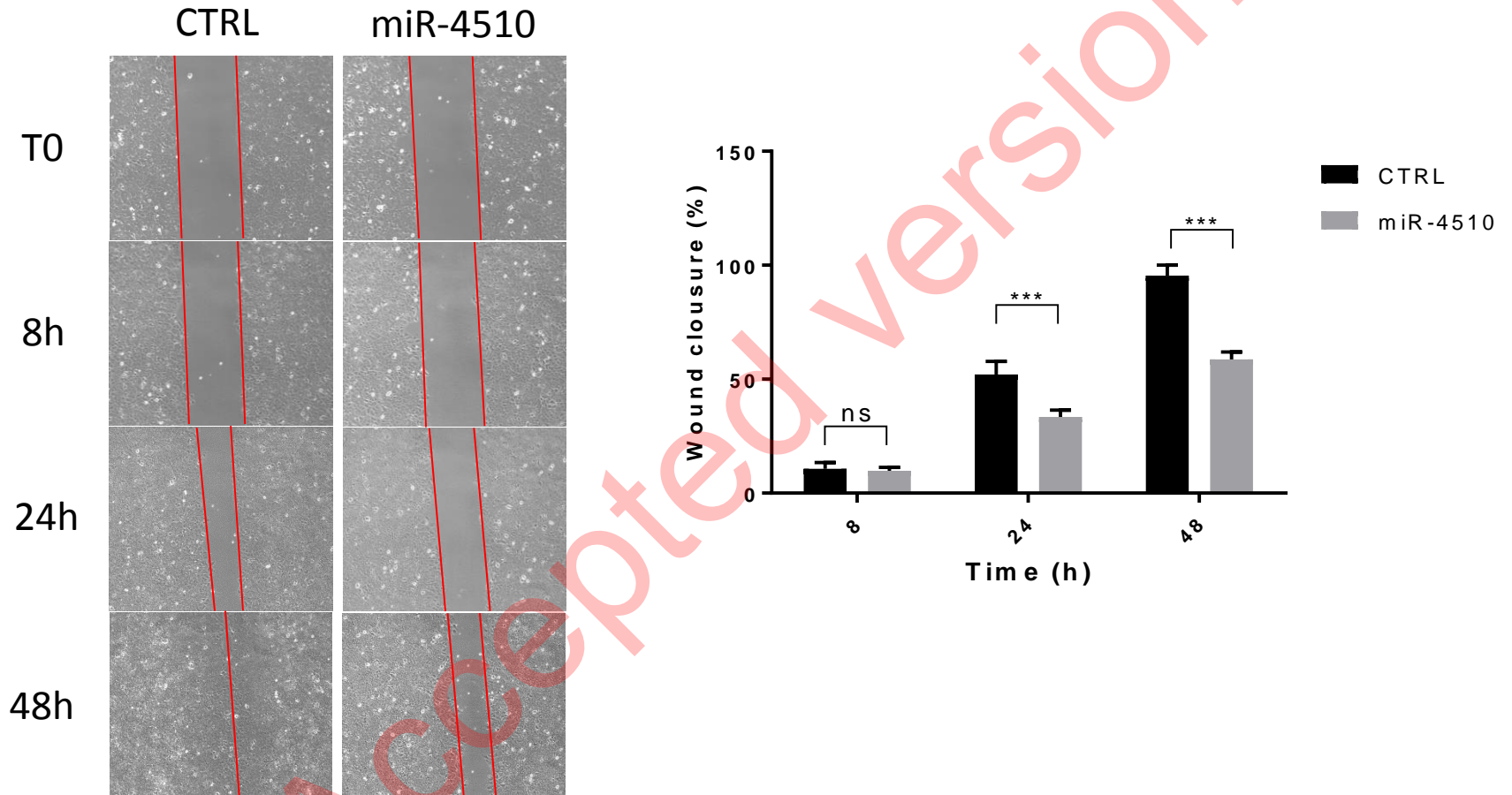
CTRL

miR-4510

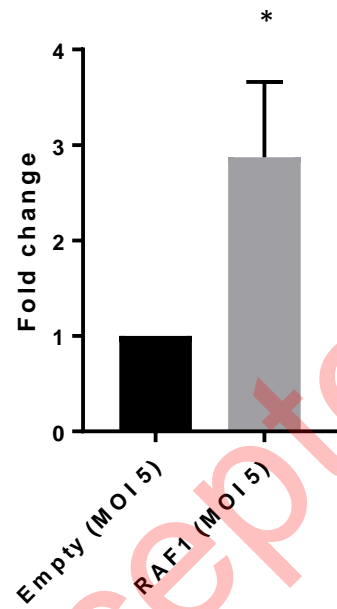
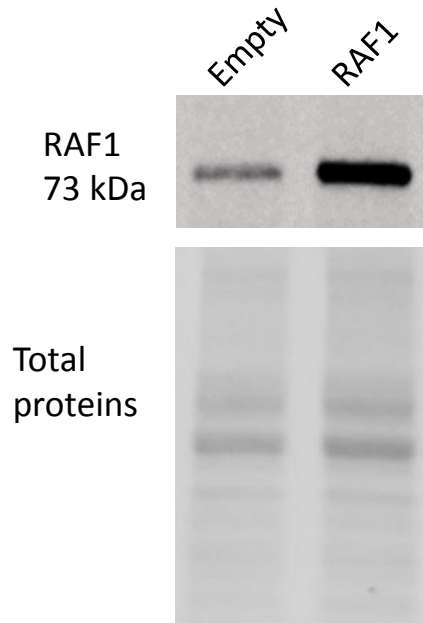
siRAF1

**b**

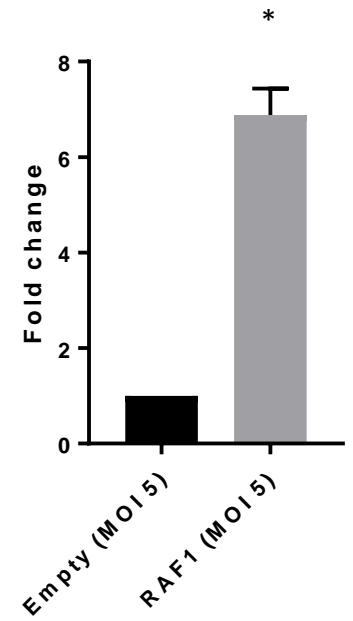
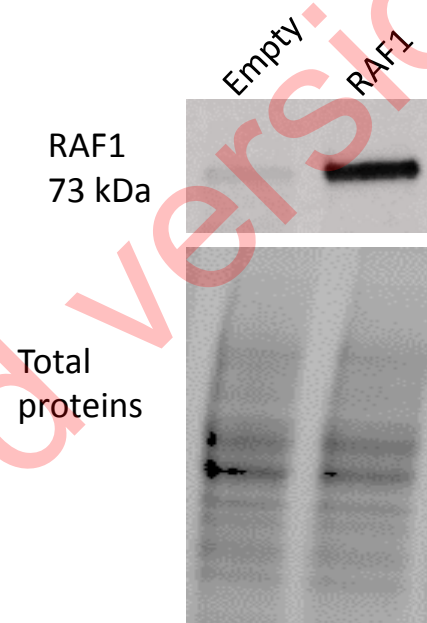
Huh7 cells



### Huh7 cells

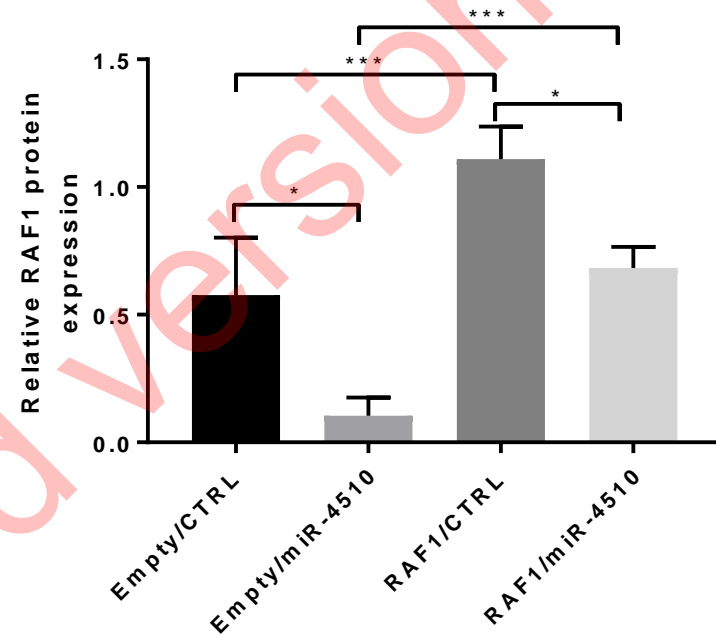
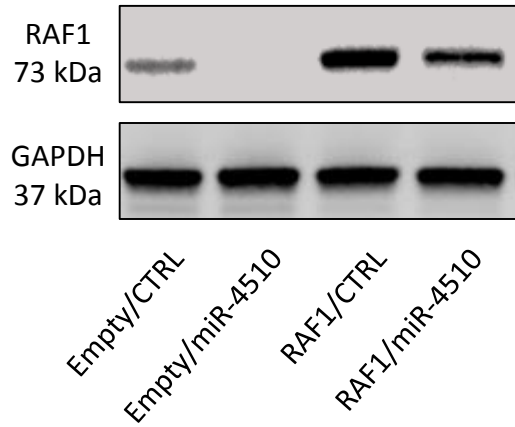


### Hep3B cells



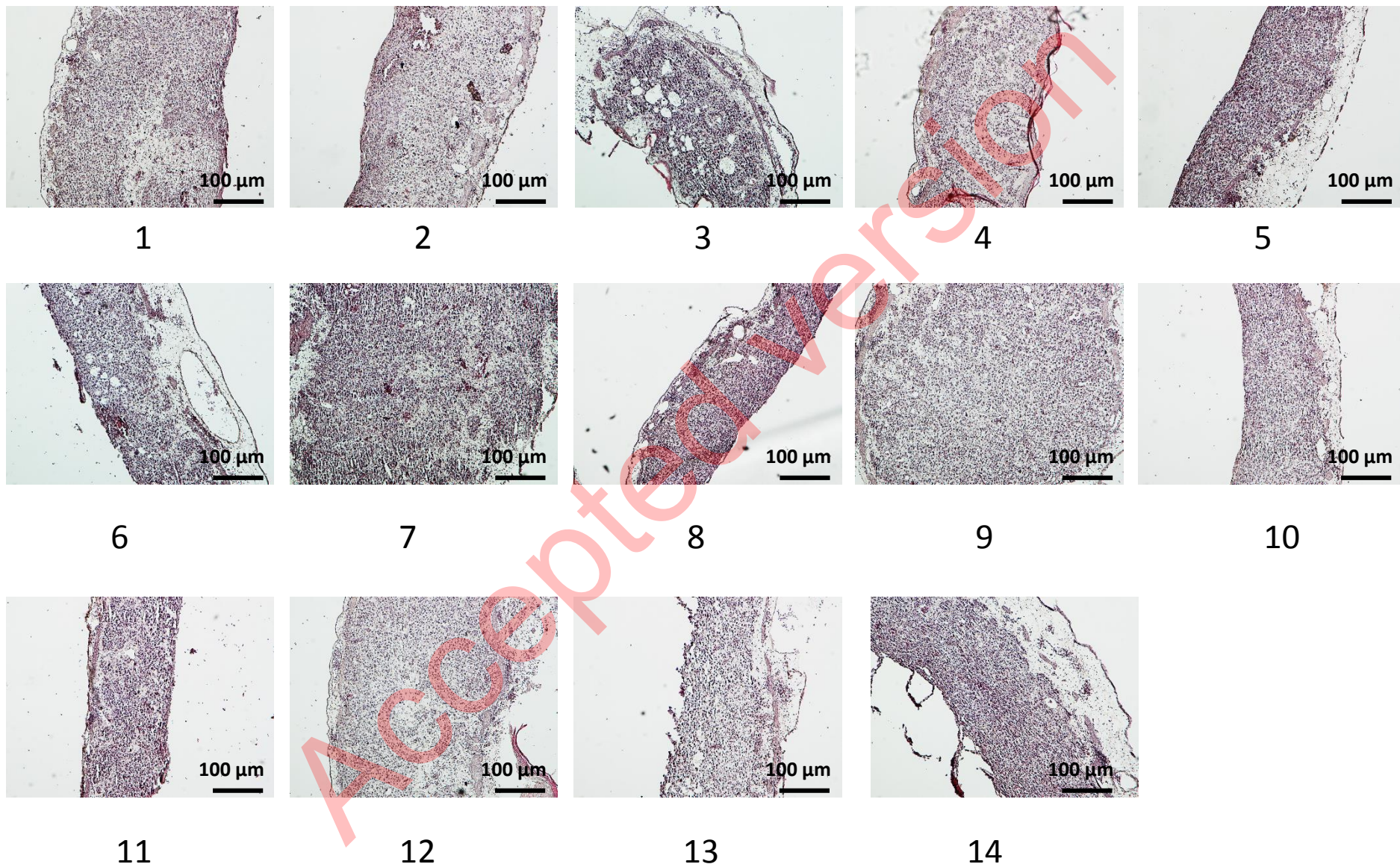
Accepted version

Huh7 cells

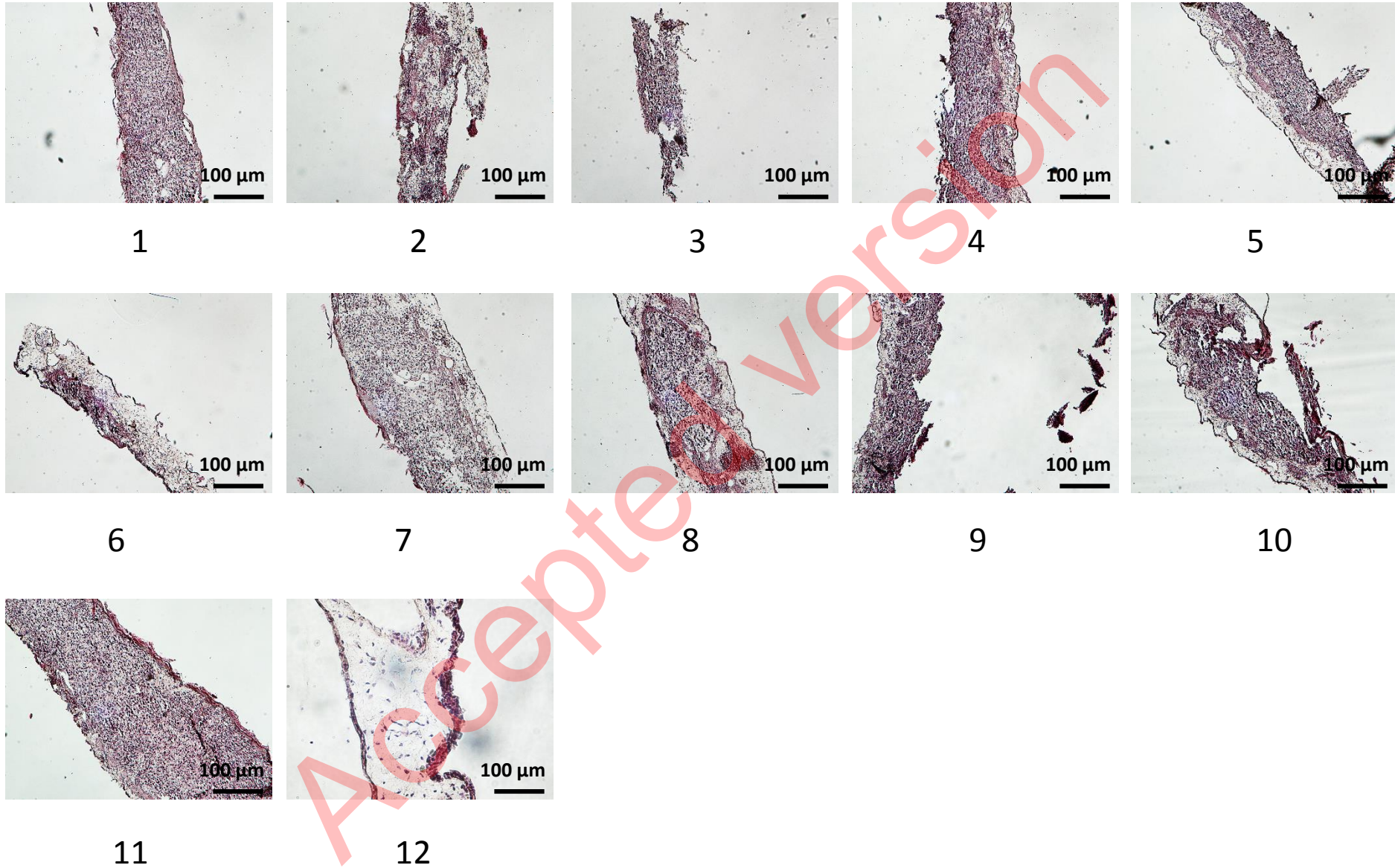


Accepted Version

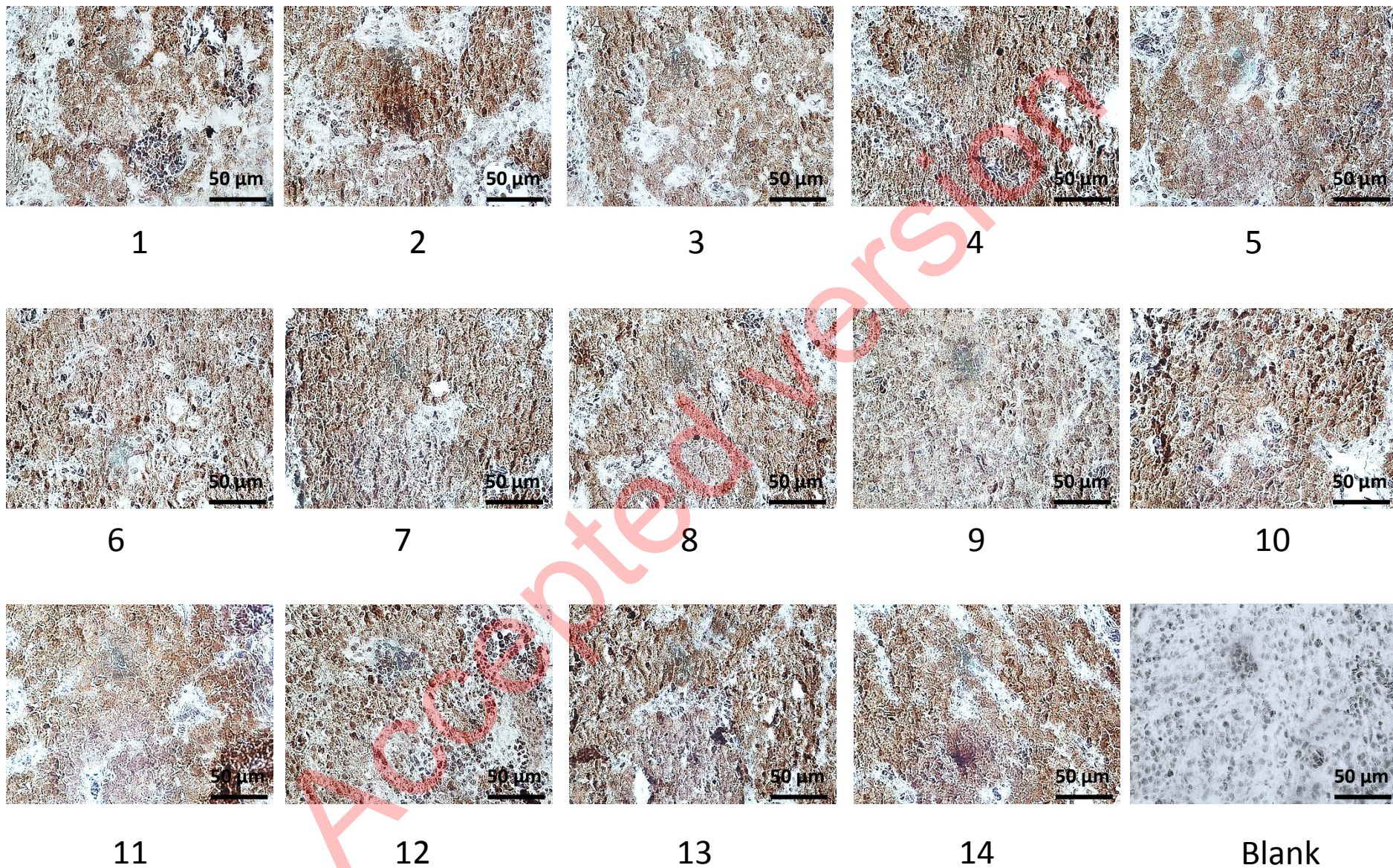
**a**



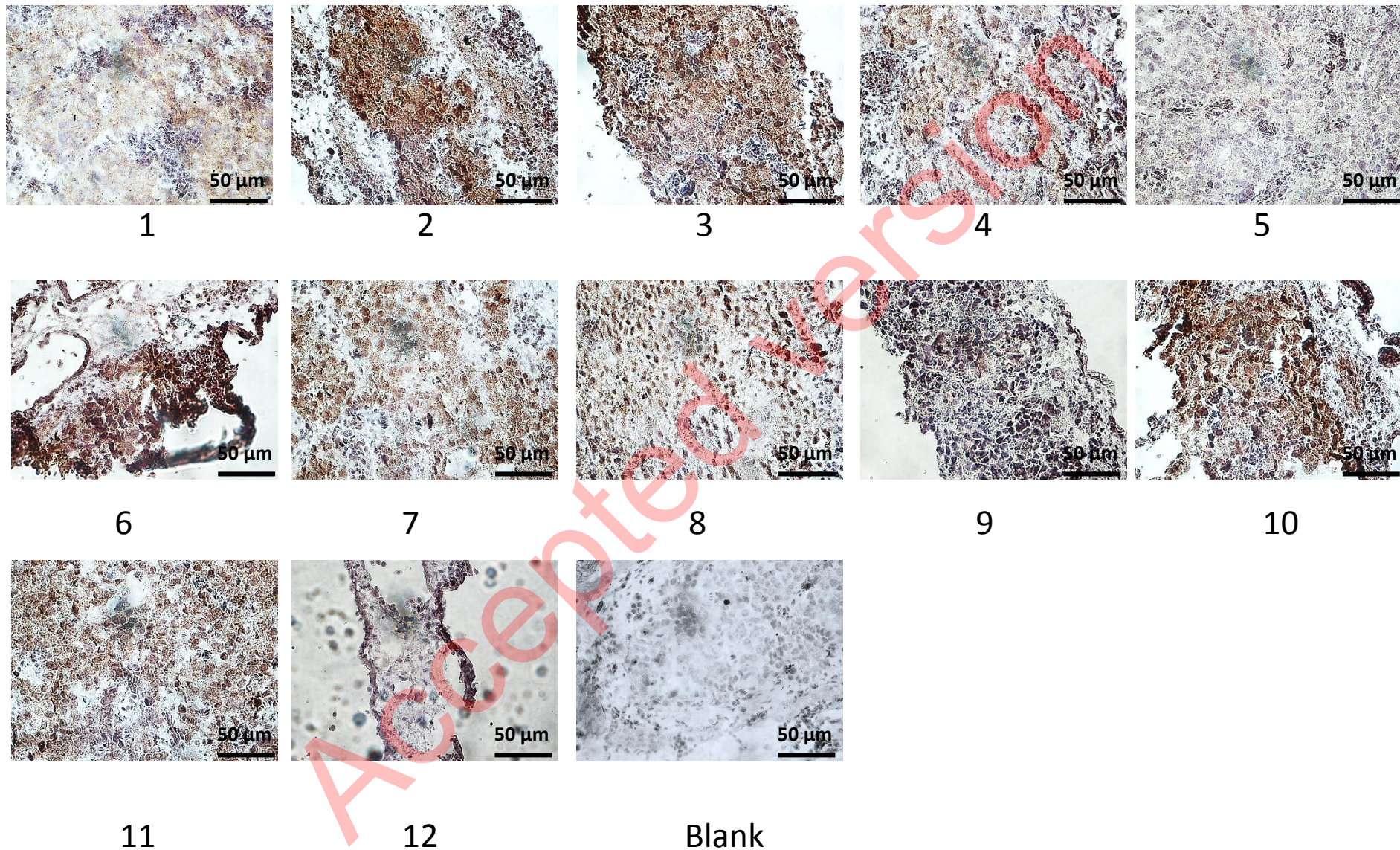
**b**



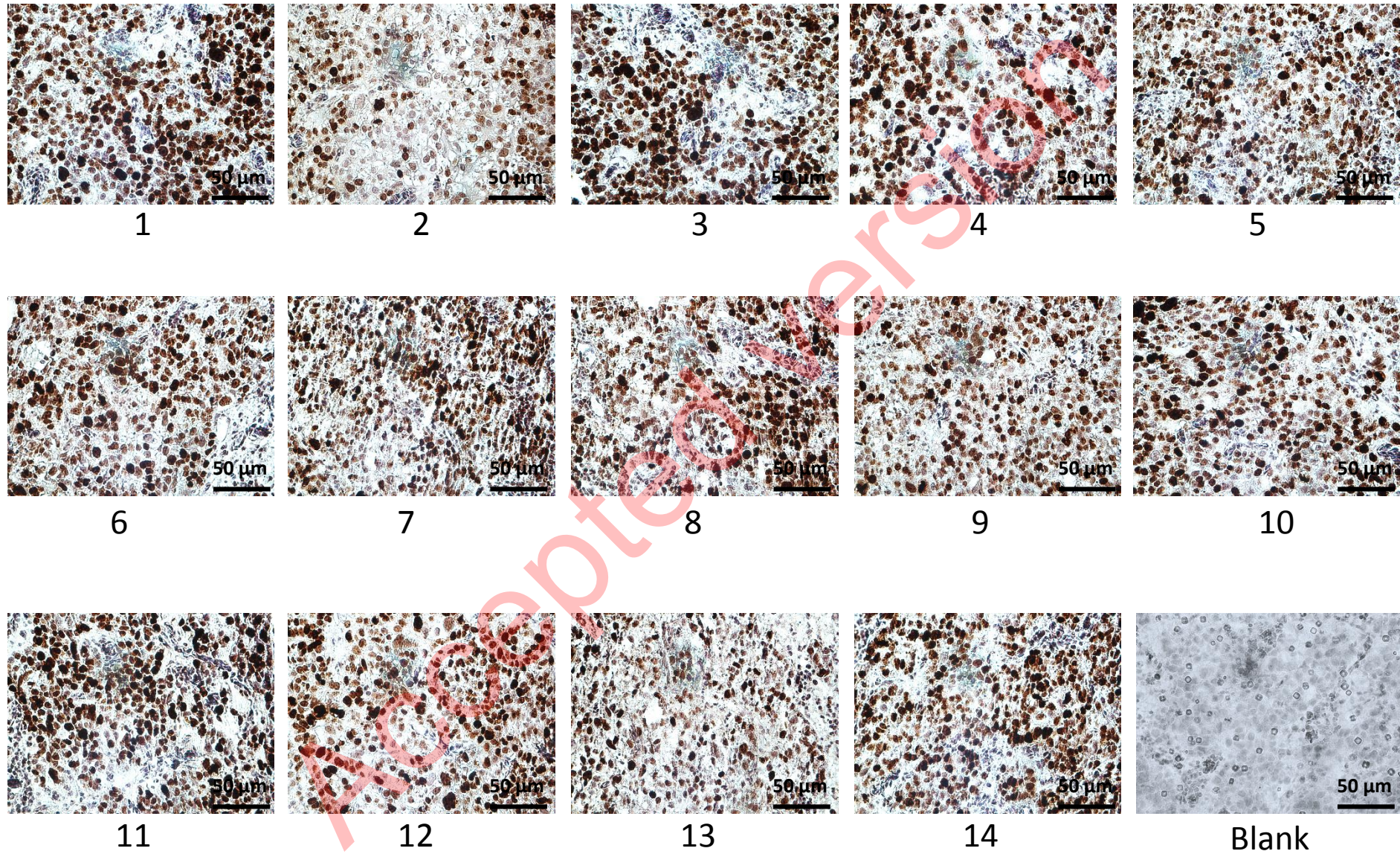
C



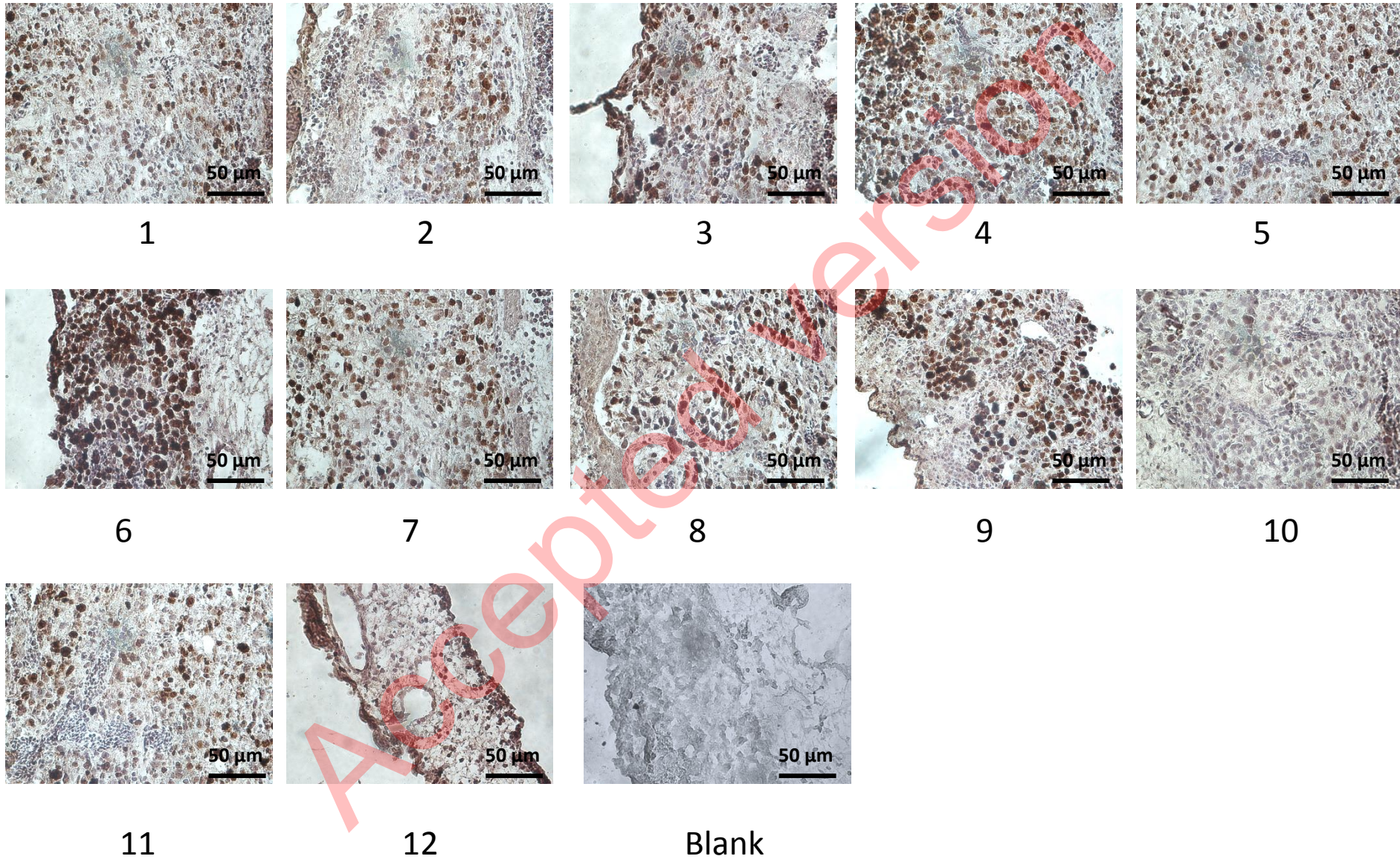
d

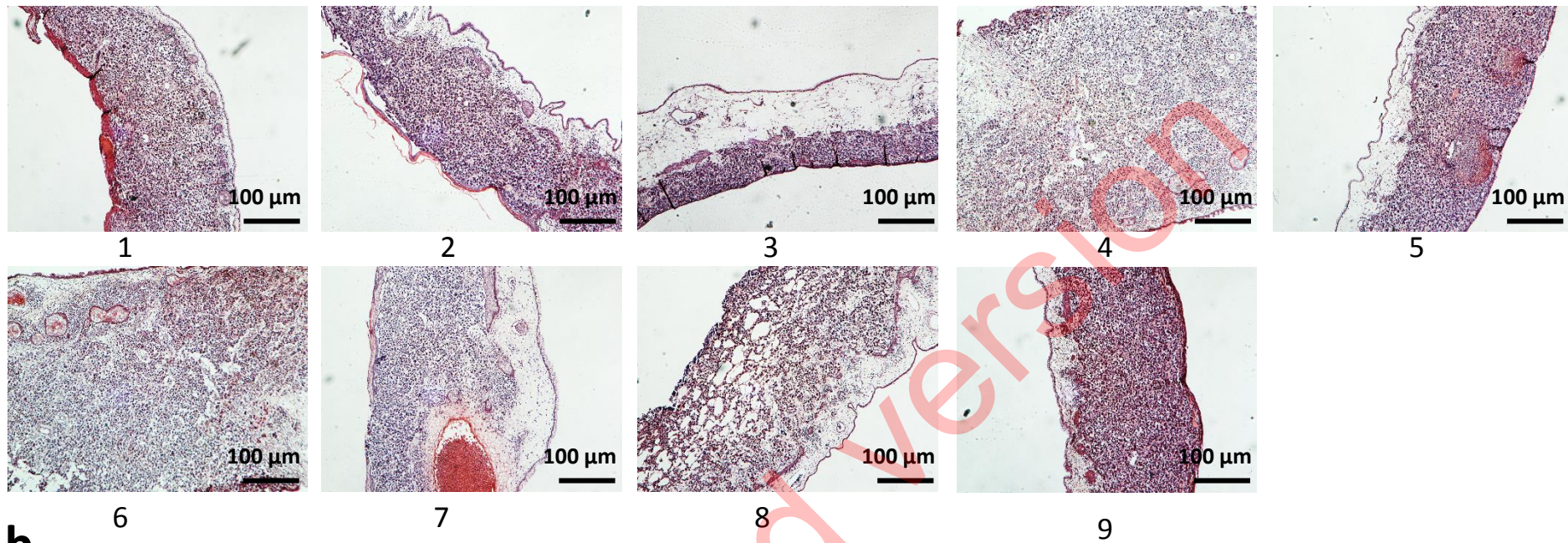
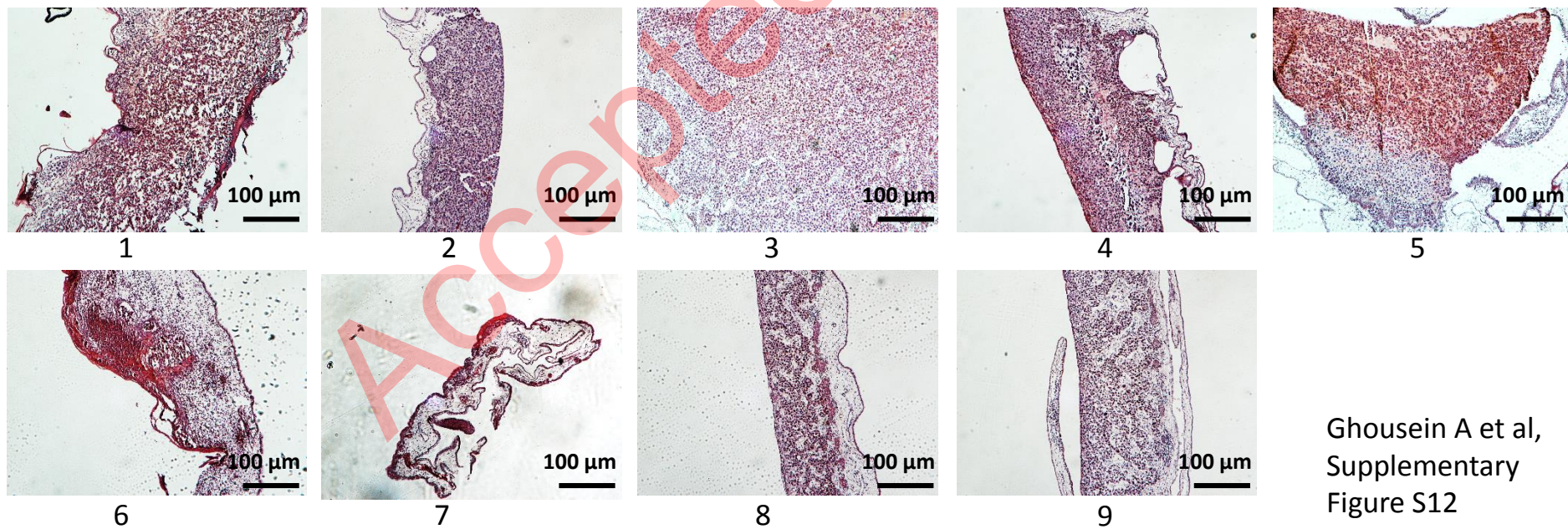


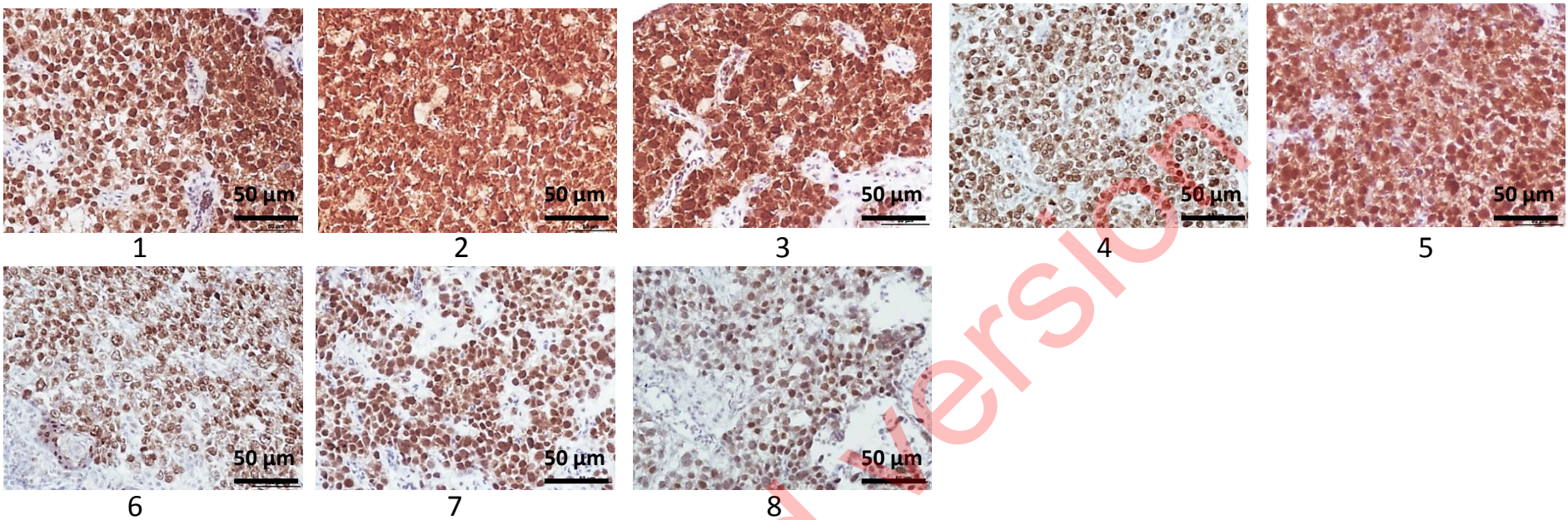
e



**f**



**a****b**

**c****d**